PHYSICAL REVIEW C **93**, 024905 (2016)

Centrality dependence of pion freeze-out radii in Pb-Pb collisions at $\sqrt{s_{NN}} = 2.76$ TeV

J. Adam *et al.**
(ALICE Collaboration)

(Received 29 July 2015; published 4 February 2016)

We report on the measurement of freeze-out radii for pairs of identical-charge pions measured in Pb-Pb collisions at $\sqrt{s_{NN}} = 2.76$ TeV as a function of collision centrality and the average transverse momentum of the pair k_{T}. Three-dimensional sizes of the system (femtoscopic radii), as well as direction-averaged one-dimensional radii are extracted. The radii decrease with k_{T}, following a power-law behavior. This is qualitatively consistent with expectations from a collectively expanding system, produced in hydrodynamic calculations. The radii also scale linearly with $\langle dN_{\mathrm{ch}}/d\eta\rangle^{1/3}$. This behavior is compared to world data on femtoscopic radii in heavy-ion collisions. While the dependence is qualitatively similar to results at smaller $\sqrt{s_{NN}}$, a decrease in the ratio $R_{\mathrm{out}}/R_{\mathrm{side}}$ is seen, which is in qualitative agreement with a specific prediction from hydrodynamic models: a change from inside-out to outside-in freeze-out configuration. The results provide further evidence for the production of a collective, strongly coupled system in heavy-ion collisions at the CERN Large Hadron Collider.

DOI: 10.1103/PhysRevC.93.024905

I. INTRODUCTION

Collisions of lead ions at $\sqrt{s_{NN}} = 2.76$ TeV have been recorded by A Large Ion Collider Experiment (ALICE) at the Large Hadron Collider (LHC) at CERN. In this energy regime, quantum chromodynamics (QCD) predicts the existence of a new state of strongly interacting matter, the quark-gluon plasma (QGP), in which quarks and gluons are no longer confined to individual nucleons. Experimental evidence for the existence of such matter has been found both at the BNL Relativistic Heavy-Ion Collider (RHIC) [1–4] as well as at the LHC [5–10]. The QGP behaves like a fluid with small viscosity and undergoes an explosive expansion. The study of the freeze-out structure and dynamics of this process may reveal important information about the matter properties, such as its equation of state and the nature of the phase transition between deconfined and ordinary hadronic matter [11,12].

Two-pion correlations at low relative momentum were first shown to be sensitive to the interaction volume of the emitting source in $\bar{p} + p$ collisions by Goldhaber *et al.* 50 years ago [13]. Since then, they were studied in $e^+ + e^-$ [14], hadron- and lepton-hadron [15], and heavy-ion [16–25] collisions. Especially in the heavy-ion case, two-particle femtoscopy has been developed into a precision tool to probe the dynamically generated spatial structure of the emitting system. In particular, a sharp phase transition between the color-deconfined and confined states was excluded by the observation of short timescales. Moreover, femtoscopic measurements, together with other observations related to bulk collective flow, provide evidence that a strongly interacting system was created in the collision [12,26,27].

Femtoscopy in heavy-ion collisions is understood in some detail; for example, see the experimental overview in Ref. [20] and model calculations in Refs. [27–30]. The dependence of the system size extracted from the data is investigated as a function of collision centrality and average transverse momentum of the pair $k_{\mathrm{T}} = |\vec{p}_{1,\mathrm{T}} + \vec{p}_{2,\mathrm{T}}|/2$. As the initial size of the system grows with increasing multiplicity (decreasing centrality), so does the apparent system size at freeze-out, measured by femtoscopy. Such increase is naturally produced in a hydrodynamic calculation. Strong hydrodynamic collective flow in the longitudinal and transverse directions results in the decrease of the apparent size of the system with increasing k_{T}. This is because longitudinal- and transverse-velocity boosts cause particles emitted from spatially separated parts of the collision region to move away from one another. Such particles cannot have a small momentum difference, and so correlation functions of boosted particles are sensitive to only part of the collision region. This part is referred to as the "homogeneity length" [31]. The decrease of the size with k_{T} is observed in experimental data from heavy-ion collisions at all centralities, various collision energies and colliding system types, and is well described quantitatively in hydrodynamic models [11,30] and qualitatively in hadronic rescattering codes [32].

Taking into account the successful description of the femtoscopic scales at lower energies, the hydrodynamic modeling has been extrapolated to collision energies of the LHC [30,33–35]. The expected increase in initial energy density (temperature) leads to larger evolution times, which in turn produce larger overall system size and stronger transverse and longitudinal flows. At the same time the freeze-out hypersurface evolves to have significant positive space-time correlation. This influences the radii of the system in the plane perpendicular to the beam axis. In particular, the radius along the pair transverse momentum (called R_{out}) is decreased by the correlation with respect to the other transverse radius (called R_{side}), which decreases the ratio $R_{\mathrm{out}}/R_{\mathrm{side}}$. All of those effects have been observed in the first measurement for central (0%–5%) collisions at the LHC [36]. This work

*Full author list given at the end of the article.

extends this measurement to other centralities and compares the obtained radii to recent hydrodynamic calculations in order to check their validity in a large range of event multiplicities. A measurement of one-dimensional radii was also performed by using the two-pion and three-pion cumulants [37]. This work extends the two-pion measurement to several ranges of pair transverse momentum.

The paper is organized as follows: In Sec. II the data-taking conditions and data treatment is described. In Sec. III we give the details of the analysis of the correlation function. In Sec. IV the extracted radii are presented and compared to model expectations, while Sec. V summarizes our findings.

II. DATA TAKING AND TRACK RECONSTRUCTION

This work reports on the analysis of Pb-Pb collisions produced by the LHC during the 2010 data-taking period. They were recorded by the ALICE experiment; the detailed description of the detector and the performance of all of its subsystems is given in Refs. [38,39]. Here we only briefly describe the specific detectors used in this analysis. The ALICE Time Projection Chamber (TPC) [40] is a large-volume gaseous ionization chamber detector, which was used both for tracking at midrapidity as well as for particle identification via the measurement of the specific ionization energy loss associated with each track. In addition to the TPC, the information from the ALICE Inner Tracker System (ITS) was used. The ITS consists of six cylindrical layers, two silicon pixel detectors closest to the beam pipe, two silicon drift detector layers in the middle, and two silicon strip detectors on the outside. The information from ITS was used for tracking and primary particle selection, as well as for triggering. However, the main triggering detector was the V0. It is a small-angle detector consisting of two arrays of 32 scintillating counters. The first (V0A) is located 330 cm from the vertex and covers $2.8 < \eta < 5.1$, the second (V0C) is fixed at the front of the hadronic absorber of the muon arm and covers $-3.7 < \eta < -1.7$. The tracking detectors are located inside the solenoidal ALICE magnet, which provides a uniform magnetic field of 0.5 T along the beam direction. The T0 detector [41] was a main luminometer in the heavy-ion run. It consists of two arrays of 12 Cherenkov counters, covering $-3.28 < \eta - 2.97$ and $4.61 < \eta < 4.92$. It has a time resolution of 40 ps.

The minimum-bias trigger required a signal in both V0 detectors, which was consistent with the collision occurring at the center of the ALICE apparatus. A total sample of approximately four million Pb-Pb events was used for this analysis. For the centrality range considered in this work the trigger efficiency was 100%. The centrality was determined by analyzing the signal from the V0 detector with the procedure described in detail in Ref. [5]. This ensured that the centrality determination was obtained by using particles at significantly different rapidities than the ones used for the pion-correlation analysis. This work presents results for seven centrality ranges: 0%–5%, 5%–10%, 10%–20%, 20%–30%, 30%–40%, 40%–50%, and 50%–60% of the total hadronic cross section. The position V_z of the event vertex in the beam direction with respect to the center of the ALICE apparatus was determined for each event. In order to ensure uniform pseudorapidity acceptance, only events with $|V_z| < 8$ cm were used in the analysis.

For each event, a list of tracks identified as primary pions was created, separately for positive and negative particles. Each track was required to leave a signal both in the TPC and the ITS and the two parts of the track had to match. The TPC is divided by the central electrode into two halves, each of them is composed of 18 sectors (covering the full azimuthal angle) with 159 pad rows placed radially in each sector. A track signal in the TPC consists of space points (clusters), each of which is reconstructed in one of the pad rows. A track was required to be composed out of at least 80 such clusters. The parameters of the track are determined by performing a Kalman fit to a set of clusters. The quality of the fit is judged by the value of χ^2, which was required to be better than 4 per cluster (each cluster has two degrees of freedom). The transverse momentum of each track was determined from its curvature in the uniform magnetic field. Two opposite field polarities were used through the data-taking period, for a check of systematic tracking effects. The momentum from this fit in the TPC was used in the analysis. Tracks which had a kink in the trajectory in the TPC were rejected. Trajectories closer than 3.2 cm in the longitudinal direction and 2.4 cm in the transverse direction to the primary vertex were selected to reduce the number of secondaries. The kinematic range for accepted particles was (0.14,2.0) GeV/c in transverse momentum and $(-0.8,0.8)$ in pseudorapidity. Based on the specific ionization energy loss in the TPC gas dE/dx, a probability for each track to be a pion, kaon, proton, or electron was determined after comparing with the corresponding Bethe–Bloch curve. Particles for which the pion probability was the largest were used in this analysis. This resulted in an overall purity above 95%, with small contamination from electrons in the region where the dE/dx curves for the two particle types intersected.

The accepted particles from each event are combined into same-charge pairs. The two-particle detector-acceptance effects must be taken into account in this procedure. Two main effects are present: track splitting and track merging. Track splitting occurs when a single trajectory is mistakenly reconstructed as two tracks. The tracking algorithm has been specifically designed to suppress such cases. In a rare event when splitting happens, two tracks are reconstructed mostly from the same clusters in the TPC. Therefore, pairs which share more than 5% of clusters are removed from the sample. Together with the antimerging cut described below, this eliminates the influence of the split pairs.

Two-particle correlated efficiency and separation power is affected by track merging. In the TPC, two tracks cannot be distinguished if their trajectories stay close to each other through a significant part of the TPC volume. Although this happens rarely, such pairs by definition have low relative momentum and therefore their absence distorts the correlation function in the signal region. The effect of track merging has been studied in central collisions in the previous work [36]. In this work we used a similar procedure to correct for the merging effects, through dedicated two-particle selection criteria. More details are given in Sec. III C.

III. CORRELATION-FUNCTION ANALYSIS

The two-particle distribution for same-event pion pairs depends on several factors, including trivial single-particle acceptance effects. To extract only the relevant two-particle correlation effects, the correlation-function formalism, described below, is applied.

A. Correlation-function construction

The femtoscopic correlation function C is constructed experimentally as

$$C(\vec{q}) = \frac{A(\vec{q})}{B(\vec{q})}, \tag{1}$$

where $\vec{q} = \vec{p}_1 - \vec{p}_2$ is the pair relative momentum (due to fixed masses of the particles only three components are independent). The magnitude of this vector is referred to as q_{inv}. For a detailed description of the formalism, see, e.g., Ref. [42]. The signal distribution A is composed of pairs of particles where both come from the same event. The background distribution B is constructed with the "mixing" method in which the two particles come from different events, which must have similar characteristics, so that their single-particle efficiency and distribution are as close as possible. To form a "mixed" pair, particles must come from two events, for which the centralities differ by no more than 2.5% and vertex positions differ by no more than 4 cm. The correlation function is normalized with the ratio of the number of pairs in the B and A samples in the full q range used (0–0.25 GeV/c), so that C at unity means no correlation. The dependence on pair momentum sum is investigated by doing the analysis for various ranges of k_{T}; namely, 0.2–0.3, 0.3–0.4, 0.4–0.5, 0.5–0.6, 0.6–0.7, 0.7–0.8, and 0.8–1.0 GeV/c. The ranges were the same for each centrality range, which overall resulted in 49 independent correlation functions per pair charge combination.

The momentum difference $\vec{q}$ is calculated in the Longitudinally Co-Moving System (LCMS), in which the pair total longitudinal momentum vanishes: $p_{1,L} + p_{2,L} = 0$. The three coordinates of $\vec{q}$ in LCMS are defined as follows: *long* - along the beam axis, *out* - along the pair transverse momentum, and *side* - perpendicular to the other two. In Fig. 1 the projections of three example correlation functions along these axes are shown. A significant, approximately Gaussian enhancement at low relative momentum is seen in all projections. The width of the correlation grows with increasing centrality (lowering multiplicity) as well as with increasing k_{T}.

The pair distributions for identical particles have specific symmetries, which are naturally represented in a spherical harmonic (SH) decomposition [43,44]. In particular, for identical particles, all odd-l and odd-m components of a correlation-function representation vanish. The gross features of the correlation function which are relevant for femtoscopy are fully captured by the low-l components of the decomposition. The $l = 0, m = 0$ component is sensitive to the overall size of the pion source. The $l = 2, m = 0$ component is sensitive to the difference between longitudinal and transverse size, and the $l = 2, m = 2$ component reflects the difference between the sideward and outward component of the transverse radius.

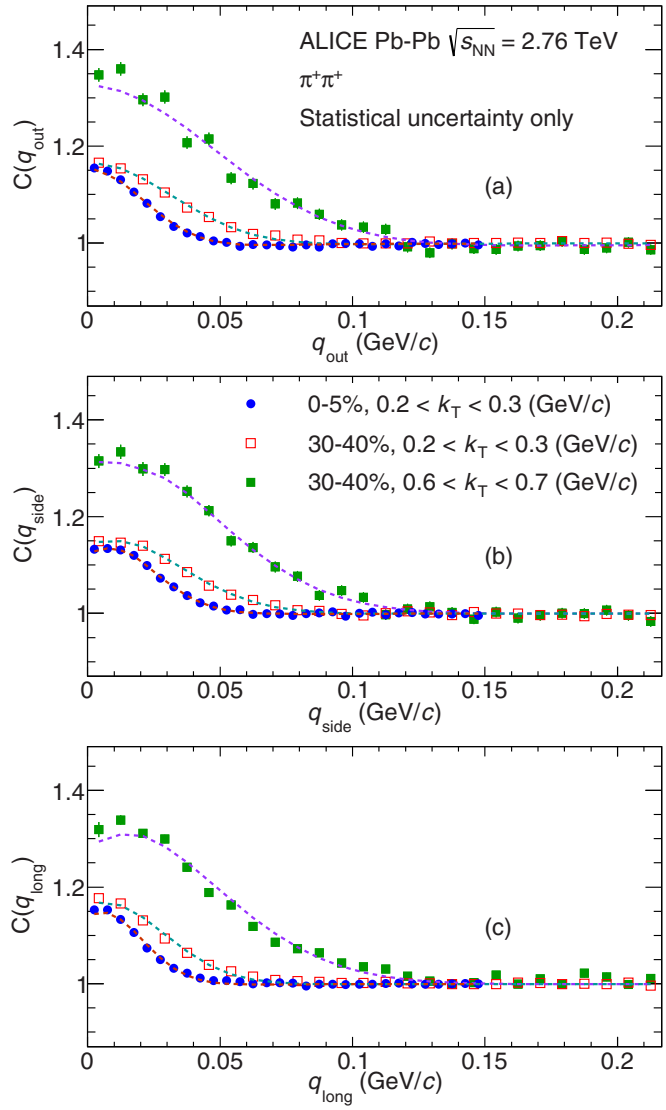

FIG. 1. Projections of the Cartesian representation of the three-dimensional two-pion correlation functions along the (a) *out*, (b) *side*, and (c) *long* axes. The centrality and pair momentum ranges for the three functions are given on the plot. In each case the other components are projected over ±20 MeV/c around 0 in the other q directions for central collisions at low k_{T} and ±33 MeV/c in the other two cases. Lines represent the corresponding projections of the fit to the experimental correlation functions with formula from Eq. (4).

Therefore, those three components of the SH representation contain the same information as the Cartesian one for the purpose of the femtoscopic analysis. In particular, both representations allow for fitting of the correlation function with the same theoretical formula. The next nonvanishing components are for $l = 4$. Their analysis is beyond the scope of this paper, which focuses on the overall width (variance) of the distribution in three directions.

In Fig. 2 we show the first three nonvanishing components of the spherical harmonics representation of three example correlation functions; the same as in Fig. 1. In the (0,0) component the enhancement at low q is clearly visible and its

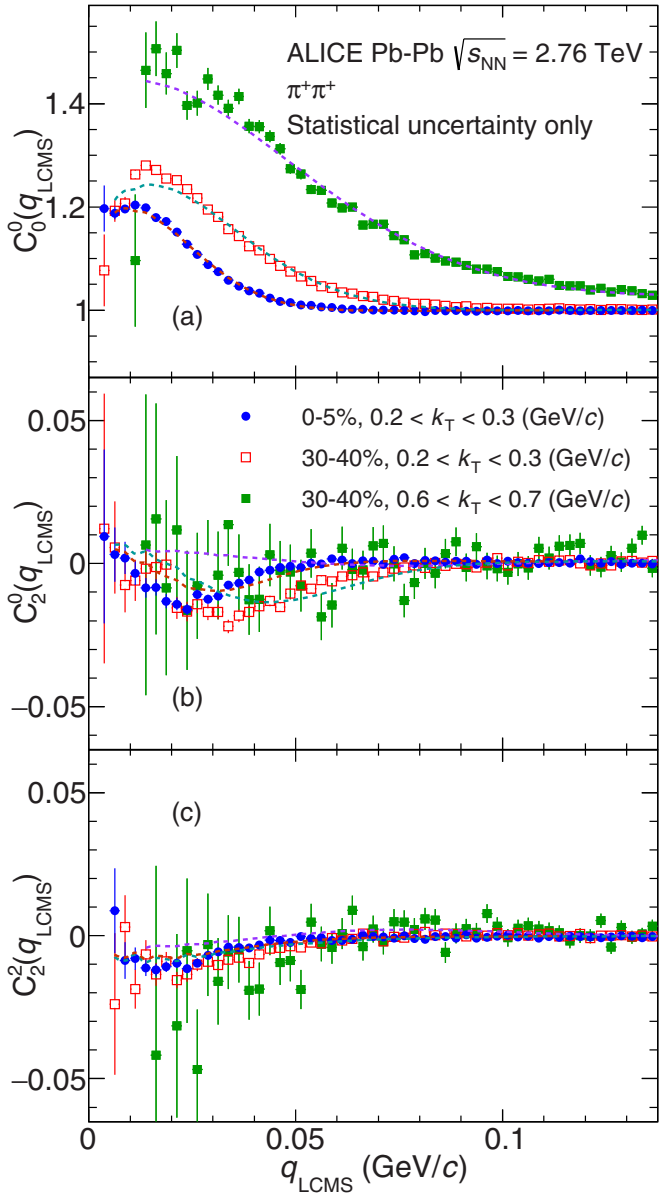

FIG. 2. First three nonvanishing components of the SH representation of the two-pion correlation functions, $l = 0$, $m = 0$ in panel (a), $l = 2$, $m = 0$ in panel (b), and $l = 2$, $m = 2$ in panel (c). The centrality and pair momentum ranges for the three functions are given on the plot. The lines show the corresponding SH components of the fit with formula from Eq. (4).

width is increasing with centrality and k_T. In this representation the low-q dip coming from Coulomb repulsion is visible better than in the Cartesian representation. For large k_T, there is a lack of low-q pairs as a result of track merging (see below). Nevertheless, the correlation clearly extends well beyond the region with low statistics. The other two components (2,0) and (2,2) show a nontrivial correlation structure deviating from zero, indicating that the shape is not spherical, but rather ellipsoidal in the LCMS. The width of these structures is consistent with the width of the correlation enhancement in the (0,0) component, which means that all three reflect the properties of the femtoscopic signal. The analysis of the shape of these structures is the main focus of the next section.

If the available statistics is limited, as is sometimes the case for lower collision energies or particles heavier than pions, the analysis is performed only as a function of magnitude of relative momentum q_{inv}, most naturally calculated in the pair rest frame (PRF). In this work we present results in this variable for completeness. Data were analyzed in the same centrality and pair k_T ranges as those used in the three-dimensional analysis.

B. Fitting the correlation function

The freeze-out characteristics of the source are reflected in the correlation function. They are connected via the Koonin–Pratt equation

$$C(\vec{q}\,) = \int S(\mathbf{r},\vec{q}\,)|\Psi(\vec{q},\mathbf{r})|^2 d^4r, \tag{2}$$

where $\mathbf{r}$ is the pair freeze-out separation four-vector. S is the source emission function, interpreted as a probability to emit a pair of particles with a given relative momentum and freeze-out separation. Ψ is the two-particle interaction kernel. In the simplest case of noninteracting particles (e.g., photons) it is the modulus of the pair wave function. If the Coulomb or strong interaction between the particles (called final-state interaction or FSI) needs to be taken into account, then Ψ becomes the Bethe–Salpeter amplitude corresponding to the solution of the relevant quantum scattering problem, taken with the inverse time direction [45].

Previous studies at the RHIC [16–18,22,23,46,47] and at the LHC [36] approximated the source by a Gaussian, treating any difference between the real data and a Gaussian as a correction. This procedure was also universally used in all past pion femtoscopic analyses of heavy-ion collisions. Therefore, we also use it here by writing

$$S(\mathbf{r},\vec{q}\,) \approx \exp\left(-\frac{r_{out}^2}{4R_{out}^2} - \frac{r_{side}^2}{4R_{side}^2} - \frac{r_{long}^2}{4R_{long}^2}\right), \tag{3}$$

where r_{out}, r_{side}, and r_{long} are components of the relative separation $\mathbf{r}$. This static form of S is expressed in the LCMS, with R_{out}, R_{side}, and R_{long} being the single-particle source sizes of the system later referred to as "femtoscopic radii," or simply "radii." They quantify the lengths of homogeneity of the system in the *outwards*, *sidewards*, and *longitudinal* directions, respectively.

For like-sign pions the strong-interaction contribution is small for the source sizes expected here (a few fm) [42], so it is neglected. The remaining Ψ is a convolution of the Coulomb interaction and wave-function symmetrization. As an approximation, the Coulomb part is factored out and integrated separately in the procedure known as the Bowler–Sinyukov fitting [48,49]. It is well tested and is applicable for pions and for the large source sizes expected in this analysis. In this approximation the integration of Eq. (2) with S given by Eq. (3) gives the following fit form for the correlation

function:

$$C(\vec{q}) = N(1-\lambda) + N\lambda K_C(q_{\rm inv})\left[1 + \exp\left(-R^2_{\rm out}q^2_{\rm out} - R^2_{\rm side}q^2_{\rm side} - R^2_{\rm long}q^2_{\rm long}\right)\right], \quad (4)$$

where N is the overall normalization factor. The function $K_C(q_{\rm inv})$ is the Coulomb part of the two-pion wave function integrated over the spherical Gaussian source with a given radius. For each correlation function it is set to the value from the one-dimensional analysis (see Sec. IV C) to reflect the decrease of the source size with multiplicity and k_T. Its variation is a source of systematic uncertainty. The dilution parameter λ is introduced to account for the fact that not all measured pion pairs are correlated, and that the real emission function may deviate from a Gaussian form.

The fit is performed with the log-likelihood method for the three-dimensional correlation function in the Cartesian representation, resulting usually in several thousand degrees of freedom. Examples are shown in Fig. 1. The Gaussian fit is able to reproduce the overall width of the correlation in all cases. Some details of the behavior at low q may not be perfectly described, which can be attributed to the limitations of the Bowler–Sinyukov formula as well as to the non-Gaussian, long-range tails which may be present in the source. Some deviations from the Gaussian ellipsoid shape for the higher centrality can also be seen for the *long* direction. We leave the detailed investigation of these effects for future work. Nevertheless, the overall sizes R of the system, which are mostly sensitive to the width of the correlation, are well estimated. The deviation of the correlation function from the pure Gaussian shape is smaller than a similar deviation in pp collisions [50].

An equivalent fit is also performed for the SH representation of the correlation. Equation (4) is numerically integrated on a φ-θ sphere for each $q_{\rm LCMS}$ bin, with proper Y_l^m weights, to produce the three components of the SH decomposition. Statistical uncertainties on each component are taken into account, as well as the covariance matrix between components. Examples are shown in Fig. 2. The fit describes the general direction-averaged width of the correlation function, shown in the upper panel of Fig. 2. Small deviations can be seen in the shape and the behavior of the fit at small q, as discussed earlier for the Cartesian fit. The deviations from zero in the (2,0) and (2,2) components are small but statistically significant for a large number of multiplicity and k_T ranges, indicating that the source size is slightly different in all three directions.

For the one-dimensional correlation functions constructed as a function of $q_{\rm inv}$, the fit was performed with a simplified version of Eq. (4):

$$C(\vec{q}) = (1-\lambda) + \lambda K_C\left[1 + \exp\left(-R^2_{\rm inv}q^2_{\rm inv}\right)\right], \quad (5)$$

where the only radius parameter is $R_{\rm inv}$—the one-dimensional direction-averaged femtoscopic radius in the PRF.

C. Systematic uncertainties of the radii

Table I lists the systematic uncertainty contributions. The range of values is given to provide a general estimate of the importance of each contribution; however, the systematic uncertainty is estimated for each point individually. Separate analyses were performed for positive and negative pions, as well as for two datasets collected with opposite polarities of the magnetic field inside ALICE. This results in four independent data samples for which certain systematic effects, most notably the single-track inefficiencies, are different. Correlation functions for all four samples for all centrality and pair momentum ranges are statistically consistent, after all corrections are applied; this is an important systematic cross-check of the methodology. In the following discussion the central values are statistical averages of the fit values obtained for the four samples. The systematic uncertainty arising from differences among the data sample is between 1% and 2% for all radii. The other systematic uncertainties are analyzed for each sample separately; their final value is the convolution of the uncertainties for each sample.

TABLE I. List of contributions to the systematic uncertainty of the extracted femtoscopic radii (ranges given).

Uncertainty source	$R_{\rm out}$ [%]	$R_{\rm side}$ [%]	$R_{\rm long}$ [%]
CF representation	0.5–5	0.5–4	0.5–8
Dataset comparison	<1.5	<1.5	<2
Fit-range dependence	0.5–4	0.5–3	1–5
Two-track cut variation	3–10	2–12	2–13
Coulomb correction	3	1	1
Momentum resolution correction	2	2	2
Centrality estimation	1	1	1
Total	6–14	4–13	4–17

Two correlation-function representations are used in this work: the Cartesian and spherical harmonics. They are mathematically equivalent; the fitting procedure used the same functional form for both. However, the implementation of the fitting procedure is quite different: log-likelihood vs regular χ^2 fit, three-dimensional Cartesian histogram vs three one-dimensional histograms, fitting range as three-dimensional cube in $q_{\rm out}$,$q_{\rm side}$,$q_{\rm long}$ or a three-dimensional sphere with constant $q_{\rm LCMS}$ radius, among others. Therefore, the fits to the two representations differ systematically upon variation of the fitting procedure (fit ranges, Bowler–Sinyukov approximation, etc.). The difference between the values for the two fits is taken as a part of the systematic uncertainty. It usually ranges from 1% to 3% and grows with pair k_T and multiplicity.

Variation of single-particle cuts around the default value results in modifications of single-particle acceptances and purities. However, the correlation-function shape should be, to first order, insensitive to those effects. We checked that, for a reasonable variation of the single-particle cuts, the resulting radii are consistent within statistical uncertainties.

The measurement of the average event multiplicity for a given centrality range has a known uncertainty of 3%–4% for all centrality classes [5]. The femtoscopic radii in heavy-ion collisions were observed to scale linearly with $\langle dN_{\rm ch}/d\eta\rangle^{1/3}$ at lower collision energies [20]. Such a trend is also predicted by hydrodynamical models and is expected to hold at the LHC. Therefore, the systematic uncertainty coming from the multiplicity estimation is about 1%.

The dominant systematic effect on the two-particle correlation function is the two-track correlated efficiency. This effect was studied in previous work [36] for central collisions. The effect of "splitting" is fully removed with the help of dedicated two-track selection criteria, mentioned in Sec. II, and does not influence the radii. However, when the trajectories of two particles are located close to each other in the volume of the TPC detector, they may be reconstructed as one track or not be reconstructed at all. This effect, called "merging" in the following, results in a loss of reconstruction efficiency for such pairs of tracks. Pairs of primary pion trajectories close in space correspond to low relative momentum, therefore merging will affect the pion correlation function exactly in the femtoscopic-signal region. The two-track efficiency was studied in Monte Carlo simulations of the ALICE detector. For pion pairs at low relative momentum, an efficiency loss of up to 20% was observed. A two-track selection was chosen, such that the resulting correlation function was not affected by the inefficiency. Merging affects only pairs which are spatially close in the detector. The "closeness" can be quantified by the pseudorapidity difference $\Delta\eta$ for the pair and only pairs with $|\Delta\eta| < 0.016$ are affected. The trajectories must also be close in the transverse plane, where they are curved by the magnetic field. The azimuthal coordinate φ^* of tracks at a radius of 1.2 m from the collision point (i.e., roughly in the center of the TPC volume) is calculated. Pairs with $(\Delta\eta^2 + \Delta\varphi^{*2})^{1/2} < 0.045$ are affected by merging. Pairs which simultaneously satisfy this and the previous angular criteria are removed both from the signal and from the background sample. The correlation function calculated for pairs surviving this cut is then not affected by merging. As a systematic check, a different procedure to calculate φ^* was used, where the value was taken not at a fixed radius, but instead at a radius inside the TPC (i.e., between 0.5 and 2.4 m) where φ^* was the smallest. The differences between radii for the correlation functions calculated with the two methods is taken as systematic uncertainty. It is from 2%–13%.

A pair of same-charge pions traversing a solenoidal field can have two configurations: a "sailor" where the two trajectories bend away from one another and never cross, or a "cowboy" where the trajectories bend toward each other and can cross [18]. Merging affects the cowboy pairs, but only weakly influences the sailors. The two configurations correspond to different phase-space regions in the Cartesian representation of the correlation function. We performed two fits to the correlations (corrected for merging), restricting the fitting range to either the cowboy or the sailor region. The consistency of the radii obtained in these fits was used as an estimator of the effectiveness of the cut for removing merged tracks. A less-restrictive cut degraded agreement between the cowboy and sailor radii, while making the cut stricter did not improve the agreement but reduced statistics in the signal region. The comparison allowed optimization of the cut and provided another estimate of the systematic uncertainty on the two-track correction procedures. The uncertainty estimated in this way is consistent with the uncertainty determined by varying the φ^* definition. This uncertainty is largest for transverse radii, is most prominent for high-multiplicity events (central collisions), and affects a wider region in q for pairs with higher k_T.

The separation into the cowboy and sailor phase-space regions is not feasible for the SH representation of the correlation function. In this case, when the antimerging cut is not properly applied, one observes significant nonfemtoscopic signals, especially in the C_2^2 component of the correlation function, and a reliable fit cannot be performed. Therefore, the C_2^2 component serves as a sensitive independent check of the effectiveness of the "antimerging" cut. This is a good illustration on how the two representations complement each other in the systematic studies.

The fit was performed for several values of the fitting range in q (varying with multiplicity and pair k_T, following the changes in the correlation-function width). The variation of the fitted radii with the change of the range was taken as another component of the uncertainty, which is less than 5% for all the radii.

In addition to the uncertainties listed above, other systematic effects can influence the extracted radii. The first is the momentum resolution, which was studied in Ref. [36]. The correction procedure described there is used in this work as well. The uncertainty on the radii from this correction is 2%. Another effect is the influence of the Bowler–Sinyukov procedure on the extracted radii and λ parameter (fraction of correlated pairs). The procedure results in an uncertainty of 3% on $R_{\rm out}$, 1% on the other radii, and lowers the λ value by up to 5% [28].

All the systematic-uncertainty components mentioned above are added in quadrature; the range of values of the total systematic uncertainty is given in Table I.

The one-dimensional analysis is performed in PRF, where the total momentum of the pair vanishes. In the transformation from LCMS to PRF $R_{\rm out}$ is scaled by the γ factor for the pair, depending on k_T, and as a consequence is larger than the other two components. In such a case, the direction-averaged one-dimensional correlation function becomes non-Gaussian. This produces a dependence of the fit value on the range of the fit, resulting in a systematic uncertainty of up to 10%. Other components of the uncertainty, such as field-orientation dependence, momentum resolution and Coulomb-correction dependence, are comparable to those from the three-dimensional fit.

IV. RESULTS

A. Three-dimensional radii

The outcome of the fitting procedure are 49 sets of femtoscopic radii, one set for each centrality and k_T range. They are shown in Figs. 3(a)–3(c). The radii in all directions are in the range of 2 to 8.5 fm. The radii universally decrease with increasing k_T, in qualitative agreement with a decreasing homogeneity length, as predicted by hydrodynamics. Such behavior is a strong indication of a large degree of collectivity in the created system. The radii are also universally higher for more central collisions, which correspond to growing final-state event multiplicity. For the lowest k_T, $R_{\rm long}$ is generally the largest, whereas at large k_T there is no universal ordering of the radii.

In the most-central collisions the values of the λ parameters are around 0.33 for the lowest k_T range, are increasing linearly

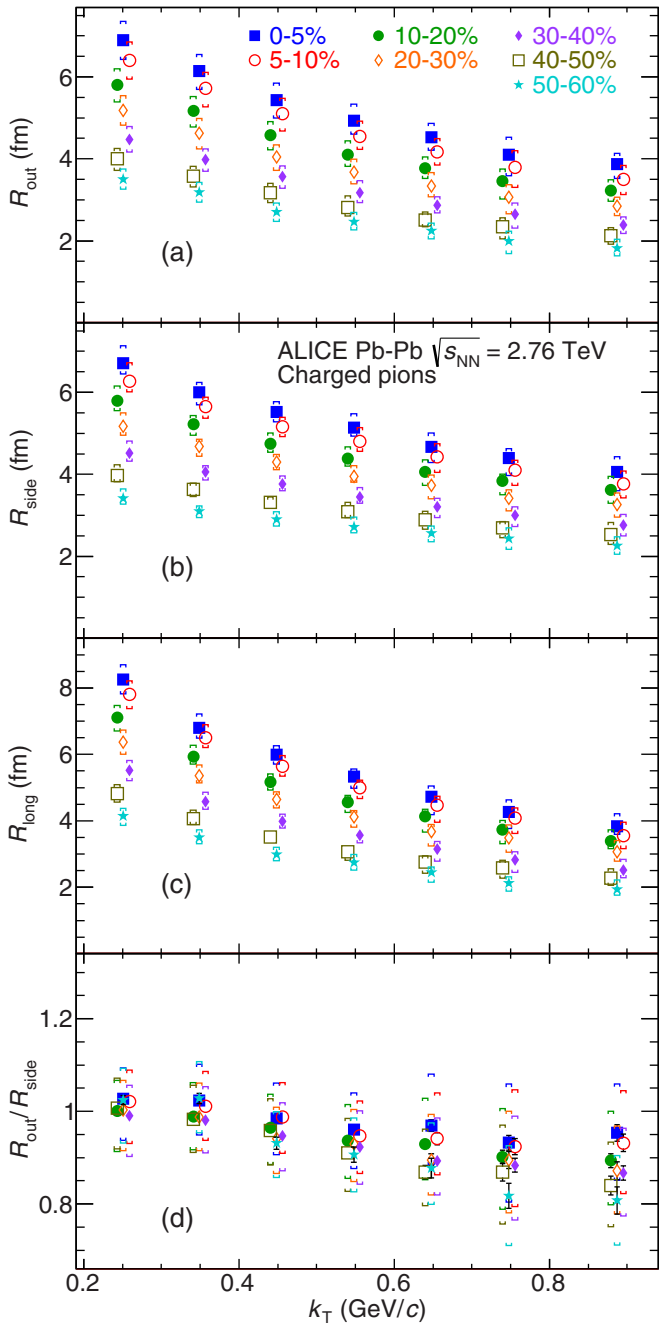

FIG. 3. Femtoscopic radii as a function of pair transverse momentum k_T for seven centrality ranges. R_{out} is shown in panel (a), R_{side} in panel (b), R_{long} in panel (c) and R_{out}/R_{side} in panel (d). The points for centralities 5%–10%, 10%–20%, 30%–40%, and 40%–50% have been slightly shifted in the x direction for visibility. Statistical uncertainties are shown as black lines (usually smaller than symbol size) and systematic uncertainties are shown as colored caps.

to 0.43 for k_T of 0.65 GeV/c, and falling to 0.36 in the last k_T range. For peripheral collisions, they are higher by 0.05 to 0.07. The lowering of λ from a theoretical maximum of 1.0 can be attributed to a number of factors. The pion sample contains daughters of long-lived strongly decaying resonances; their fraction falls with growing p_T. As a result the source function contains non-Gaussian tails extending to large relative separation. There may be additional factors influencing the shape of the correlation function, coming from the source dynamics. The exact source shape usually deviates from a Gaussian in a way that lowers the λ parameter of the Gaussian fit significantly. The detailed study of this shape requires a dedicated methodology and is beyond the scope of this work. In addition, at the largest k_T the electron and pion dE/dx become comparable in the TPC, and the pion sample is contaminated by electrons, which also lowers λ. The approximate treatment of the Coulomb interaction in the Bowler–Sinyukov fitting procedure lowers it by 5%–10% [28]. This effect is most pronounced for large source sizes (central collisions). Finally, possible coherent emission of pions [51] is expected to lower λ by a few percent. The λ-parameter values given here are for reference only and their physics interpretation is not discussed.

In panel Fig. 3(d) the ratio R_{out}/R_{side} is shown. Its systematic uncertainty is determined independently from those of R_{out} and R_{side} to account for the fact that they may be correlated. The ratio is consistent with unity for central collisions. Its value slowly decreases for more peripheral collisions and reaches 0.85 for peripheral collisions and high k_T. Based on hydrodynamic models, the ratio R_{out}/R_{side} was proposed as a sensitive probe of the shape and space-time correlation present at the freeze-out hypersurface [33,52]. In particular, this ratio at the LHC was predicted to be lower than the value of 1.1 measured at top RHIC collision energies.

B. Scaling of the radii

It was argued in Ref. [20] that the femtoscopic volume scales with the final-state event multiplicity, and that each of the three-dimensional radii separately scales with this value taken to the power 1/3. In Fig. 4 we present the dependence of the radii on multiplicity for Pb-Pb collisions. The scaling is evident for all datasets, for all three directions, and all analyzed pair momentum ranges.

Similarly, hydrodynamics predicts approximate scaling of the radii with pair transverse mass $m_T = (k_T^2 + m_\pi^2)^{1/2}$ [35]. The slope parameters of the lines shown in Fig. 4 are plotted in Fig. 5 as a function of m_T. They are fit with a power-law function of the form

$$a(m_T) = \beta \left(\frac{m_T}{m_\pi} \right)^{\alpha}, \tag{6}$$

where β and α are free parameters. The slope parameters follow the power-law scaling within the current systematic uncertainties; the value of the α parameter is -0.65 ± 0.12 for the *long* direction, -0.46 ± 0.13 for the *out* direction, and -0.52 ± 0.11 for the *side* direction. The dependence of the values of femtoscopic radii on centrality and k_T factorizes into a linear dependence on $\langle dN_{ch}/d\eta \rangle^{1/3}$ and a power-law dependence on m_T.

C. One-dimensional analysis

The results of the one-dimensional fits with Eq. (5) are shown in Fig. 6. Similarly to the three-dimensional case, the radius is increasing with event multiplicity (decreasing centrality). Therefore, the final-state shape is reflecting the

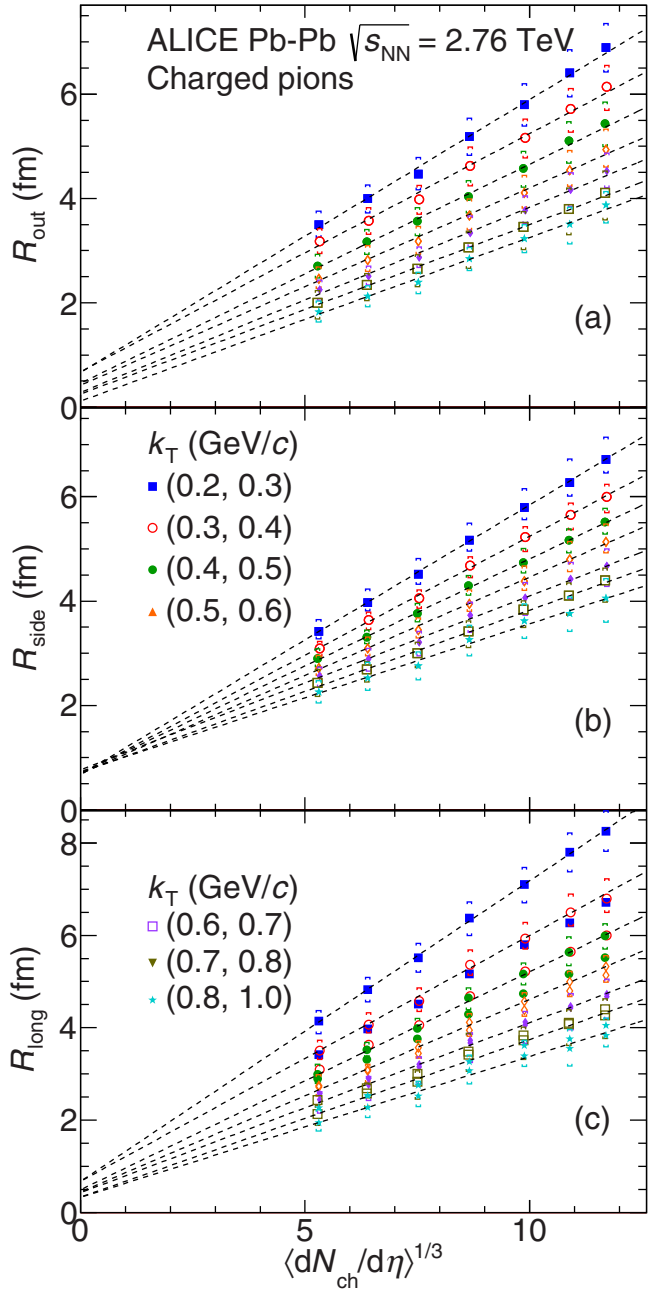

FIG. 4. The radii plotted as a function of $\langle dN_{ch}/d\eta \rangle^{1/3}$ for seven k_T ranges. R_{out} is plotted in panel (a), R_{side} in panel (b), and R_{long} in panel (c). The dashed lines represent linear fits to each set of points for a given component and k_T range. Points for some k_T ranges have been slightly shifted in the x direction for visibility. Statistical uncertainties are shown as black lines (usually smaller than symbol size), systematic uncertainties are shown as colored caps.

growth of the initial shape with decreasing centrality. R_{inv} is also decreasing with pair transverse momentum. This is usually understood as a manifestation of the hydrodynamic collectivity. The one-dimensional radius also serves as a comparison basis with the femtoscopic analysis for heavier particles, where the one-dimensional analysis is standard and the three-dimensional analysis is challenged by the more

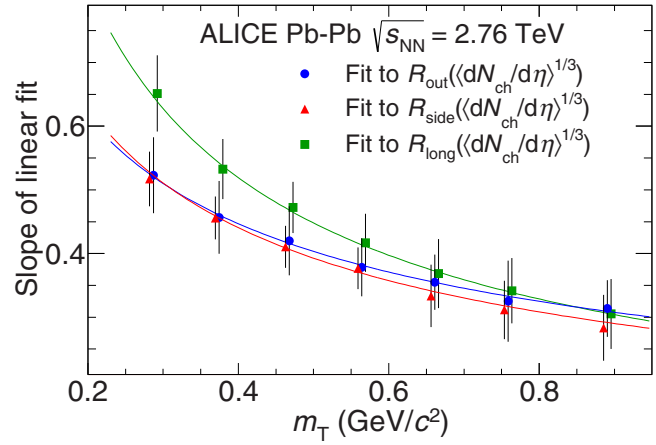

FIG. 5. The slope parameters of the linear fits shown in Fig. 4 as a function of pair m_T. Lines represent the power-law fits (see text for details). Error bars represent the uncertainty of the parameter of the fits, in which the combined systematic and statistical uncertainties on the radii were taken into account.

complicated description of the pair interaction as well as significantly smaller statistics [54,55].

D. Comparison to previous measurements

In Fig. 7 the heavy-ion data from Pb-Pb collisions at the LHC reported in this work are compared with the previous measurements, including results obtained at lower collision energies. It has been argued [20] that three-dimensional femtoscopic radii scale with the cube root of measured charged-particle multiplicity not only for a single energy and collision system, but universally, across all collision energies and initial system sizes. The dashed lines in the figure are linear fits to heavy-ion data available before the startup of

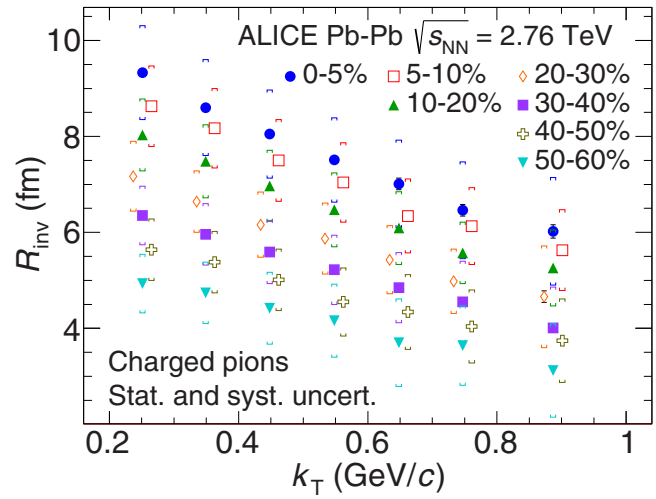

FIG. 6. One-dimensional femtoscopic radius R_{inv} as a function of pair transverse momentum k_T for seven centrality ranges. Points for 5%–10%, 20%–30%, and 40%–50% centrality have been slightly shifted in the x direction for visibility. Statistical uncertainty is shown as black lines, systematic uncertainty is shown as colored caps.

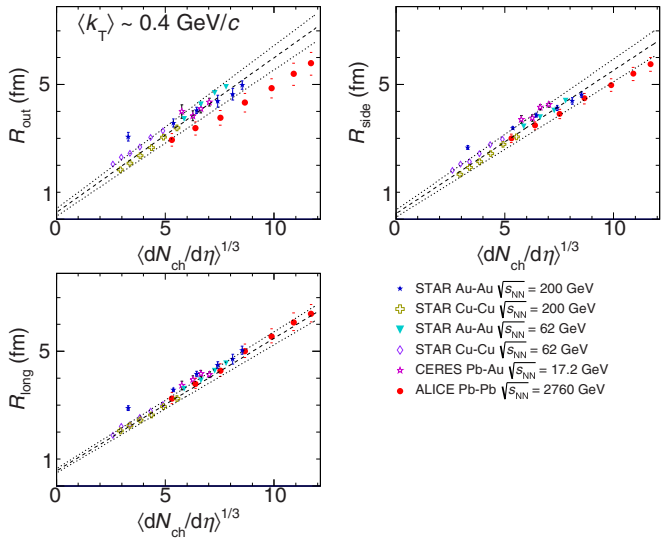

FIG. 7. Comparison of femtoscopic radii as a function of measured charged-particle multiplicity, for a number of collision systems and collision energies [18,46,53]. Dashed lines show linear fits done to heavy-ion data, excluding ALICE (dotted lines show one-sigma contour). Various experiments use differing k_T ranges; values shown on the plot are for the range for which the average k_T is closest to the selected value of 0.4 GeV/c; in case of ALICE an average of two neighboring ranges of k_T is shown. Systematic uncertainties are shown where available.

the LHC (the dotted lines show one-sigma contours of these fits). At lower energies the linear scaling was followed well in *long* and *side* directions and only approximately in *out*, with some outliers such as the most peripheral collisions reported by STAR. Our data at higher collision energy show that the scaling in the *long* direction is preserved. The data for the *side* direction fall below the scaling trend, although still within the statistical uncertainty. A clear departure from the linear scaling is seen in the *out* direction; data from the LHC lie clearly below the trend from lower energies. Such behavior was predicted by hydrodynamic calculations [33] and is the result of the modification of the freeze-out shape. Larger initial deposited energy produces larger temperature gradients and longer evolution time at the LHC. This results in a change from outside-in to inside-out freeze-out and this modification of the space-time correlation drives the ratio $R_{\rm out}/R_{\rm side}$ to values lower than at the RHIC. Therefore, already for heavy-ion data the simple universal linear scaling is broken in the transverse direction. As already reported in Ref. [50], the femtoscopic radii for pp collisions also exhibit linear scaling in the same variable, albeit with significantly different parameters. In this case the scaling between different colliding systems is broken again in the longitudinal direction.

Other scaling variables were proposed for the femtoscopic radii, based on Monte Carlo simulations of the initial state, such as average number of participants $N_{\rm part}$ [46] or the characteristic initial transverse size $\bar{R}$ [56,57]. If data from different centralities but the same collision energy are considered, a linear scaling is indeed observed for radii in all directions, if they are plotted as a function of either of these variables. However, no such scaling is observed when data from two collision energies (e.g., top RHIC and top LHC) are compared. In that sense these variables are less adequate than $\langle dN_{\rm ch}/d\eta\rangle^{1/3}$, for which the linear scaling is preserved, across many collision energies, for at least one direction ($R_{\rm long}$). This observation is consistent with an expectation that the final freeze-out volume, reflected in the femtoscopic radii, should scale with the final-state observable (such as, e.g., $\langle dN_{\rm ch}/d\eta\rangle^{1/3}$), while the simple "geometric" initial-state variables do not contain enough information. They must be replaced with modeling of the full evolution process, such as the one given by hydrodynamics, which depends on additional parameters apart from the initial size, such as initial energy density.

E. Model comparisons

The hydrodynamic models predict both the centrality and pair momentum dependence of the femtoscopic radii. Usually the parameters of the model (initial energy-density profile, the equation of state, and the freeze-out condition) are adjusted to reproduce the shape of the single-particle inclusive transverse momentum spectra as well as the elliptic flow. The charged-particle multiplicity must also be reproduced, preferably as a function of pseudorapidity if the model employs full three-dimensional modeling. The total particle multiplicity is usually determined on the freeze-out hypersurface by employing statistical hadronization. After converting the continuous medium to hadrons, final-state interactions are taken into account either in the simplified form, with propagation and decay of hadronic resonances or with the full rescattering simulation. We compare our results to predictions from the Therminator model coupled to $(3+1)$-dimensional [$(3+1)$D] viscous hydrodynamics [34,35,58]. Similar results have been obtained in the hydrokinetic model (HKM) [30].

In Fig. 8 we show the comparison of our data to the calculations from the $(3+1)$D hydrodynamic model coupled to the Therminator statistical hadronization code. The model is fully three dimensional and is able to reproduce values of $R_{\rm long}$ for all centralities, with some overprediction of the overall magnitude and the slope of the k_T dependence, especially at low momentum. This is an indication that the longitudinal dynamics is reasonably described in the model, both in momentum and space-time sectors. $R_{\rm out}$ is well described for all centralities, both in magnitude as well in the slope of the k_T dependence. The slope of the k_T dependence is also well described for $R_{\rm side}$, but the magnitude is lower than in data, although within the systematic uncertainty. The intercept of $R_{\rm side}$ at low k_T is usually associated with the overall geometrical size of the system, while the slope of the k_T dependence of both transverse radii depends on the amount of flow in the system. Both are well reproduced, so the hydrodynamic approach is in good agreement with our data.

Another model based on hydrodynamic formalism, the HKM [30], is also shown in Fig. 8 for the 0%–5% most-central collisions. It differs from the previous model in the implementation of the freeze-out process. It also directly treats hadron rescattering with the UrQMD simulation. Nevertheless, the pion femtoscopy in central Pb-Pb collisions at the LHC is reproduced in the calculation, with some underprediction

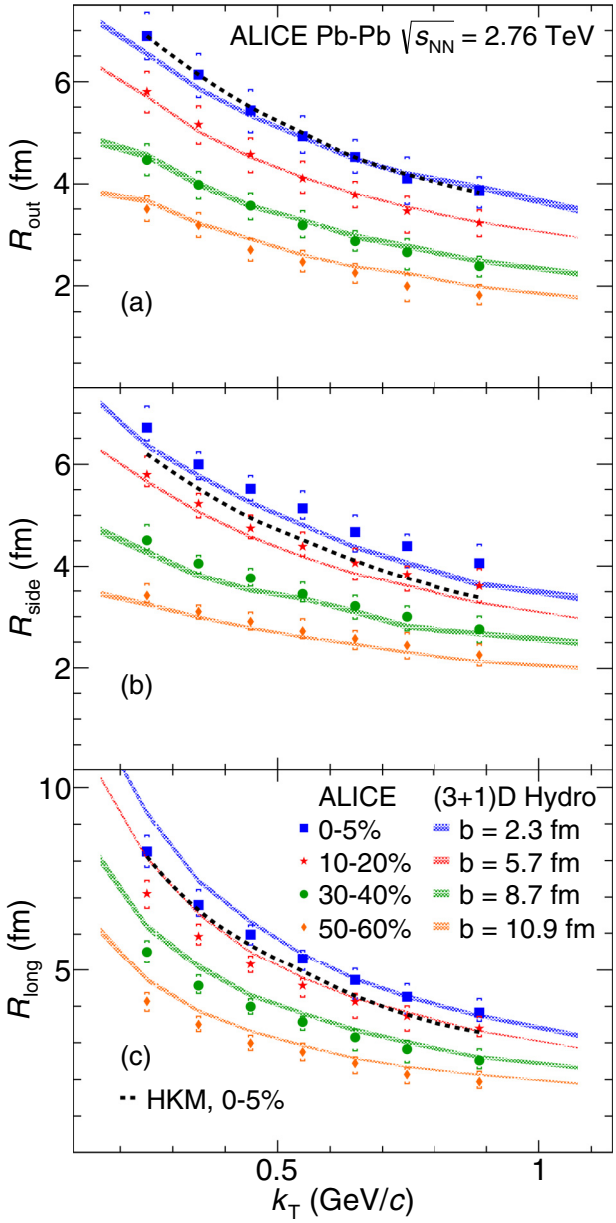

FIG. 8. Comparison of the femtoscopic radii [R_{out} in panel (a), R_{side} in panel (b), and R_{long} in panel (c)] as a function of pair transverse momentum, with the calculation from the Therminator and (3 + 1)D hydro model [35], for four centralities (here identified by the value of the impact parameter b used in the calculation) and with the HKM model [30] for the central data. Closed symbols are experimental data (with statistical and systematic uncertainty), bands and dashed lines are the model calculations.

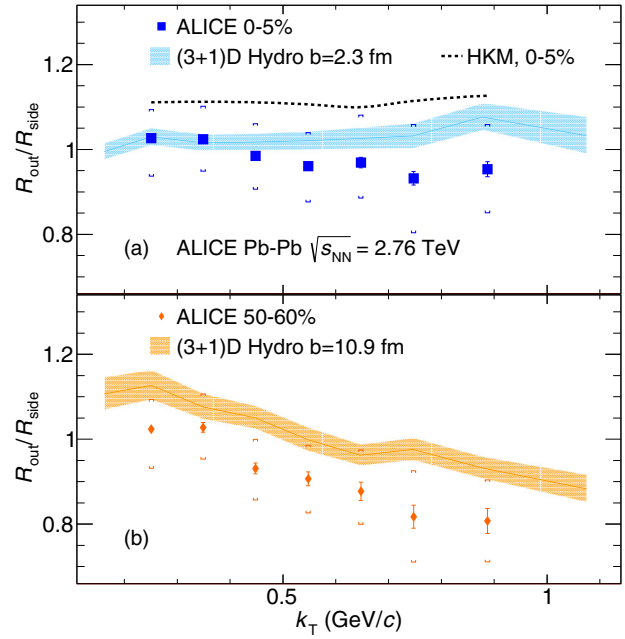

FIG. 9. Comparison of the ratio R_{out}/R_{side} as a function of pair transverse momentum, with the calculation from the Therminator and (3 + 1)D hydro model [35], for 0%–5% centrality in panel (a) and 50%–60% centrality in panel (b). The comparison to the HKM model [30] is also shown for the central data. Closed symbols are experimental data (with statistical and systematic uncertainty), bands and dashed lines are the model calculations.

of R_{side} and R_{long} magnitude. Therefore, the approximate agreement with data is a universal feature of such models, not of a particular implementation. The particular choice of initial conditions and the equation of state for these models was motivated by the analysis of the RHIC femtoscopic data. This choice is essential for the correct description of the data, which is due to the collective-flow mechanism in the hydrodynamic evolution at the LHC energies. It also indicates that the details of the freeze-out process have limited influence on pion femtoscopy. Some studies suggest that femtoscopy of heavier particles might be a more sensitive probe in this case [30].

The data to model comparison of the R_{out}/R_{side} ratio is plotted in Fig. 9. It shows values consistent with unity for central collisions, both for models and data. Such low values are associated with the change to outside-in freeze-out scenario at LHC collision energies. For most peripheral collisions the ratio decreases with k_T even more to values smaller than unity. This decrease is qualitatively reproduced in the model, although the calculations are at the upper edge of the experimental systematic uncertainty.

V. CONCLUSIONS

We report on the centrality and pair k_T dependence of the three-dimensional and direction-averaged one-dimensional pion femtoscopic radii in Pb-Pb collisions at $\sqrt{s_{NN}} =$ 2.76 TeV. The behavior of the femtoscopic radii can be factorized into a linear dependence on the cube root of charged-particle density (separately for each of the three-dimensional radii) and a power-law dependence on pair transverse momentum, with slightly different exponents for each direction. The dependence for the longitudinal radius is steeper than for the transverse ones. The dependence was also compared to that observed in heavy-ion collisions at lower energies and to other collisions systems. The radii at the LHC follow the "universal" $\langle dN_{ch}/d\eta \rangle^{1/3}$ scaling in the *long* direction, but the radii in the transverse directions are below the universal

curve. Simple linear scaling predictions are not valid when the collision energy is increased by an order of magnitude. The details of the dynamic evolution of the system influence the results significantly. This is in qualitative agreement with predictions from hydrodynamic models. In particular, when moving from the RHIC to the LHC collision energies, they produce a change in freeze-out shape, larger transverse radial flow, and longer system-evolution time. Comparison of the full dataset to the calculations from the recent hydrodynamic models, including three-dimensional evolution as well as hadronic stage, generally show a good agreement, which is complementary to similar agreement observed for momentum-only observables, such as momentum spectra and elliptic flow. The existence of such agreement both in the space-time as well as in momentum sectors provides strong arguments for the validity of hydrodynamic models for the description of flowing bulk matter created in heavy-ion collisions at the LHC.

ACKNOWLEDGMENTS

The ALICE Collaboration would like to thank all its engineers and technicians for their invaluable contributions to the construction of the experiment and the CERN accelerator teams for the outstanding performance of the LHC complex. The ALICE Collaboration gratefully acknowledges the resources and support provided by all Grid centres and the Worldwide LHC Computing Grid (WLCG) collaboration. The ALICE Collaboration acknowledges the following funding agencies for their support in building and running the ALICE detector: State Committee of Science, World Federation of Scientists (WFS) and Swiss Fonds Kidagan, Armenia; Conselho Nacional de Desenvolvimento Científico e Tecnológico (CNPq), Financiadora de Estudos e Projetos (FINEP), Fundação de Amparo á Pesquisa do Estado de São Paulo (FAPESP); National Natural Science Foundation of China (NSFC), the Chinese Ministry of Education (CMOE) and the Ministry of Science and Technology of China (MSTC); Ministry of Education and Youth of the Czech Republic; Danish Natural Science Research Council, the Carlsberg Foundation and the Danish National Research Foundation; The European Research Council under the European Community's Seventh Framework Programme; Helsinki Institute of Physics and the Academy of Finland; French CNRS-IN2P3, the 'Region Pays de Loire', 'Region Alsace', 'Region Auvergne' and CEA, France; German Bundesministerium fur Bildung, Wissenschaft, Forschung und Technologie (BMBF) and the Helmholtz Association; General Secretariat for Research and Technology, Ministry of Development, Greece; National Research, Development and Innovation Office (NKFIH), Hungary; Department of Atomic Energy and Department of Science and Technology of the Government of India; Istituto Nazionale di Fisica Nucleare (INFN) and Centro Fermi - Museo Storico della Fisica e Centro Studi e Ricerche "Enrico Fermi", Italy; Japan Society for the Promotion of Science (JSPS) KAKENHI and MEXT, Japan; Joint Institute for Nuclear Research, Dubna; National Research Foundation of Korea (NRF); Consejo Nacional de Cienca y Tecnologia (CONACYT), Direccion General de Asuntos del Personal Academico(DGAPA), México, Amerique Latine Formation academique - European Commission (ALFA-EC) and the EPLANET Program (European Particle Physics Latin American Network); Stichting voor Fundamenteel Onderzoek der Materie (FOM) and the Nederlandse Organisatie voor Wetenschappelijk Onderzoek (NWO), Netherlands; Research Council of Norway (NFR); National Science Centre, Poland; Ministry of National Education/Institute for Atomic Physics and National Council of Scientific Research in Higher Education (CNCSI-UEFISCDI), Romania; Ministry of Education and Science of Russian Federation, Russian Academy of Sciences, Russian Federal Agency of Atomic Energy, Russian Federal Agency for Science and Innovations and The Russian Foundation for Basic Research; Ministry of Education of Slovakia; Department of Science and Technology, South Africa; Centro de Investigaciones Energeticas, Medioambientales y Tecnologicas (CIEMAT), E-Infrastructure shared between Europe and Latin America (EELA), Ministerio de Economía y Competitividad (MINECO) of Spain, Xunta de Galicia (Consellería de Educación), Centro de Aplicaciones Tecnológicas y Desarrollo Nuclear (CEADEN), Cubaenergía, Cuba, and IAEA (International Atomic Energy Agency); Swedish Research Council (VR) and Knut & Alice Wallenberg Foundation (KAW); Ukraine Ministry of Education and Science; United Kingdom Science and Technology Facilities Council (STFC); The United States Department of Energy, the United States National Science Foundation, the State of Texas, and the State of Ohio; Ministry of Science, Education and Sports of Croatia and Unity through Knowledge Fund, Croatia; Council of Scientific and Industrial Research (CSIR), New Delhi, India; Pontificia Universidad Católica del Perú.

[1] J. Adams *et al.* (STAR Collaboration), Experimental and theoretical challenges in the search for the quark gluon plasma: The STAR Collaboration's critical assessment of the evidence from RHIC collisions, Nucl. Phys. A **757**, 102 (2005).

[2] K. Adcox *et al.* (PHENIX Collaboration), Formation of dense partonic matter in relativistic nucleus nucleus collisions at RHIC: Experimental evaluation by the PHENIX Collaboration, Nucl. Phys. A **757**, 184 (2005).

[3] B. B. Back *et al.* (PHOBOS Collaboration), The PHOBOS perspective on discoveries at RHIC, Nucl. Phys. A **757**, 28 (2005).

[4] I. Arsene *et al.* (BRAHMS Collaboration), Quark gluon plasma and color glass condensate at RHIC? The perspective from the BRAHMS experiment, Nucl. Phys. A **757**, 1 (2005).

[5] K. Aamodt *et al.* (ALICE Collaboration), Centrality dependence of the charged-particle multiplicity density at midrapidity in Pb-Pb collisions at $\sqrt{s_{NN}} = 2.76$ TeV, Phys. Rev. Lett. **106**, 032301 (2011).

[6] K. Aamodt *et al.* (ALICE Collaboration), Elliptic flow of charged particles in Pb-Pb collisions at 2.76 TeV, Phys. Rev. Lett. **105**, 252302 (2010).

[7] B. Abelev *et al.* (ALICE Collaboration), Anisotropic flow of charged hadrons, pions, and (anti-)protons measured at high transverse momentum in Pb-Pb collisions at $\sqrt{s_{\rm NN}} = 2.76$ TeV, Phys. Lett. B **719**, 18 (2013).

[8] K. Aamodt *et al.* (ALICE Collaboration), Suppression of charged-particle production at large transverse momentum in central Pb-Pb collisions at $\sqrt{s_{NN}} = 2.76$ TeV, Phys. Lett. B **696**, 30 (2011).

[9] G. Aad *et al.* (ATLAS Collaboration), Observation of a centrality-dependent dijet asymmetry in lead-lead collisions at $\sqrt{s_{NN}} = 2.77$ TeV with the ATLAS detector at the LHC, Phys. Rev. Lett. **105**, 252303 (2010).

[10] S. Chatrchyan *et al.* (CMS Collaboration), Observation and studies of jet quenching in Pb-Pb collisions at nucleon-nucleon center-of-mass energy = 2.76 TeV, Phys. Rev. C **84**, 024906 (2011).

[11] W. Broniowski, M. Chojnacki, W. Florkowski, and A. Kisiel, Uniform description of soft observables in heavy-ion collisions at $\sqrt{s_{\rm NN}} = 200$ GeV, Phys. Rev. Lett. **101**, 022301 (2008).

[12] S. Pratt, The long slow death of the HBT puzzle, Proceedings for QM 2009, Nucl. Phys. A **830**, 51c (2009).

[13] G. Goldhaber, S. Goldhaber, W.-Y. Lee, and A. Pais, Influence of Bose–Einstein statistics on the antiproton proton annihilation process, Phys. Rev. **120**, 300 (1960).

[14] W. Kittel, Bose-Einstein correlations in Z fragmentation and other reactions, Acta Phys. Pol. B **32**, 3927 (2001).

[15] G. Alexander, Bose–Einstein and Fermi–Dirac interferometry in particle physics, Rep. Prog. Phys. **66**, 481 (2003).

[16] C. Adler *et al.* (STAR Collaboration), Pion interferometry of $\sqrt{s_{\rm NN}} = 130$ GeV Au + Au collisions at RHIC, Phys. Rev. Lett. **87**, 082301 (2001).

[17] J. Adams *et al.* (STAR Collaboration), Azimuthally sensitive HBT in Au + Au collisions at $\sqrt{s_{\rm NN}} = 200$ GeV, Phys. Rev. Lett. **93**, 012301 (2004).

[18] J. Adams *et al.* (STAR Collaboration), Pion interferometry in Au + Au collisions at $\sqrt{s_{\rm NN}} = 200$ GeV, Phys. Rev. C **71**, 044906 (2005).

[19] S. S. Adler *et al.* (PHENIX Collaboration), Bose–Einstein correlations of charged-pion pairs in Au + Au collisions at $\sqrt{s_{\rm NN}} = 200$ GeV, Phys. Rev. Lett. **93**, 152302 (2004).

[20] M. Lisa, S. Pratt, R. Soltz, and U. Wiedemann, Femtoscopy in relativistic heavy-ion collisions, Annu. Rev. Nucl. Part. Sci. **55**, 357 (2005).

[21] B. Abelev *et al.* (STAR Collaboration), Neutral kaon interferometry in Au + Au collisions at $\sqrt{s_{\rm NN}} = 200$ GeV, Phys. Rev. C **74**, 054902 (2006).

[22] S. S. Adler *et al.* (PHENIX Collaboration), Evidence for a long-range component in the pion emission source in Au + Au collisions at $\sqrt{s_{\rm NN}} = 200$ GeV, Phys. Rev. Lett. **98**, 132301 (2007).

[23] S. Afanasiev *et al.* (PHENIX Collaboration), Source breakup dynamics in Au + Au collisions at $\sqrt{s_{\rm NN}} = 200$ GeV via three-dimensional two-pion source imaging, Phys. Rev. Lett. **100**, 232301 (2008).

[24] S. Afanasiev *et al.* (PHENIX Collaboration), Kaon interferometric probes of space-time evolution in Au + Au collisions at $\sqrt{s_{\rm NN}} = 200$ GeV, Phys. Rev. Lett. **103**, 142301 (2009).

[25] A. Adare *et al.* (PHENIX Collaboration), Azimuthal-angle dependence of charged-pion-interferometry measurements with respect to 2$^{\rm nd}$- and 3$^{\rm rd}$-order event planes in Au + Au collisions at $\sqrt{s_{NN}} = 200$ GeV, Phys. Rev. Lett. **112**, 222301 (2014).

[26] D. Hardtke and S. A. Voloshin, The relationship between particle freeze-out distributions and HBT radius parameters, Phys. Rev. C **61**, 024905 (2000).

[27] M. Chojnacki, W. Florkowski, W. Broniowski, and A. Kisiel, Soft heavy-ion physics from hydrodynamics with statistical hadronization: Predictions for collisions at $\sqrt{s_{\rm NN}} = 5.5$ TeV, Phys. Rev. C **78**, 014905 (2008).

[28] A. Kisiel, W. Florkowski, and W. Broniowski, Femtoscopy in hydro-inspired models with resonances, Phys. Rev. C **73**, 064902 (2006).

[29] R. Soltz, I. Garishvili, M. Cheng, B. Abelev, A. Glenn *et al.*, Constraining the initial temperature and shear viscosity in a hybrid hydrodynamic model of $\sqrt{s_{\rm NN}} = 200$ GeV Au + Au collisions using pion spectra, elliptic flow, and femtoscopic radii, Phys. Rev. C **87**, 044901 (2013).

[30] I. Karpenko, Y. Sinyukov, and K. Werner, Uniform description of bulk observables in hydrokinetic model of $A + A$ collisions at the BNL Relativistic Heavy Ion Collider and the CERN Large Hadron Collider, Phys. Rev. C **87**, 024914 (2013).

[31] S. V. Akkelin and Y. M. Sinyukov, The HBT interferometry of expanding sources, Phys. Lett. B **356**, 525 (1995).

[32] Q. Li, G. Graef, and M. Bleicher, UrQMD calculations of two-pion HBT correlations in $p + p$ and Pb + Pb collisions at LHC energies, J. Phys.: Conf. Ser. **420**, 012039 (2013).

[33] A. Kisiel, W. Broniowski, M. Chojnacki, and W. Florkowski, Azimuthally-sensitive femtoscopy from RHIC to LHC in hydrodynamics with statistical hadronization, Phys. Rev. C **79**, 014902 (2009).

[34] P. Bozek, Flow and interferometry in $(3 + 1)$-dimensional viscous hydrodynamics, Phys. Rev. C **85**, 034901 (2012).

[35] A. Kisiel, M. Galazyn, and P. Bozek, Pion, kaon, and proton femtoscopy in Pb-Pb collisions at $\sqrt{s_{\rm NN}} = 2.76$ TeV modeled in $(3 + 1)$D hydrodynamics, Phys. Rev. C **90**, 064914 (2014).

[36] K. Aamodt *et al.* (ALICE Collaboration), Two-pion Bose-Einstein correlations in central Pb-Pb collisions at $\sqrt{s_{\rm NN}} =$ 2.76 TeV, Phys. Lett. B **696**, 328 (2011).

[37] B. B. Abelev *et al.* (ALICE Collaboration), Freeze-out radii extracted from three-pion cumulants in pp, p-Pb and Pb-Pb collisions at the LHC, Phys. Lett. B **739**, 139 (2014).

[38] K. Aamodt *et al.* (ALICE Collaboration), The ALICE experiment at the CERN LHC, JINST **3**, S08002 (2008).

[39] B. B. Abelev *et al.* (ALICE Collaboration), Performance of the ALICE Experiment at the CERN LHC, Int. J. Mod. Phys. A **29**, 1430044 (2014).

[40] J. Alme, Y. Andres, H. Appelshauser, S. Bablok, N. Bialas *et al.*, The ALICE TPC, a large three-dimensional tracking device with fast readout for ultra-high multiplicity events, Nucl. Instrum. Methods Phys. Res., Sect. A **622**, 316 (2010).

[41] M. Bondila, V. Grigorev, F. Guber, V. Kaplin, A. Karakash *et al.*, ALICE T0 detector, IEEE Trans. Nucl. Sci. **52**, 1705 (2005).

[42] R. Lednicky, Correlation femtoscopy, Nucl. Phys. A **774**, 189 (2006).

[43] Z. Chajecki, Femtoscopy in hadron and lepton collisions: RHIC results and world systematics, Acta Phys. Pol. B **40**, 1119 (2009).

[44] A. Kisiel and D. A. Brown, Efficient and robust calculation of femtoscopic correlation functions in spherical harmonics directly from the raw pairs measured in heavy-ion collisions, Phys. Rev. C **80**, 064911 (2009).

[45] R. Lednicky, Finite-size effects on two-particle production in continuous and discrete spectrum, Phys. Part. Nucl. **40**, 307 (2009).
[46] B. I. Abelev *et al.* (STAR Collaboration), Pion interferometry in Au + Au and Cu + Cu collisions at $\sqrt{s_{\rm NN}} = 62.4$ and 200 GeV, Phys. Rev. C **80**, 024905 (2009).
[47] K. Adcox *et al.* (PHENIX Collaboration), Transverse mass dependence of two-pion correlations in Au + Au collisions at $\sqrt{s_{\rm NN}} = 130$ GeV, Phys. Rev. Lett. **88**, 192302 (2002).
[48] M. G. Bowler, Coulomb corrections to Bose–Einstein correlations have been greatly exaggerated, Phys. Lett. B **270**, 69 (1991).
[49] Y. Sinyukov, R. Lednicky, S. V. Akkelin, J. Pluta, and B. Erazmus, Coulomb corrections for interferometry analysis of expanding hadron systems, Phys. Lett. B **432**, 248 (1998).
[50] K. Aamodt *et al.* (ALICE Collaboration), Femtoscopy of *pp* collisions at $\sqrt{s} = 0.9$ and 7 TeV at the LHC with two-pion Bose-Einstein correlations, Phys. Rev. D **84**, 112004 (2011).
[51] B. B. Abelev *et al.* (ALICE Collaboration), Two- and three-pion quantum statistics correlations in Pb-Pb collisions at $\sqrt{s_{NN}} = 2.76$ TeV at the CERN Large Hadron Collider, Phys. Rev. C **89**, 024911 (2014).
[52] I. Karpenko and Y. Sinyukov, Energy dependence of pion interferometry scales in ultrarelativistic heavy-ion collisions, Phys. Lett. B **688**, 50 (2010).
[53] D. Adamova *et al.* (CERES Collaboration), Beam energy and centrality dependence of two-pion Bose–Einstein correlations at SPS energies, Nucl. Phys. A **714**, 124 (2003).
[54] B. Abelev *et al.* (ALICE Collaboration), K^0_s-K^0_s correlations in *pp* collisions at $\sqrt{s} = 7$ TeV from the LHC ALICE experiment, Phys. Lett. B **717**, 151 (2012).
[55] B. Abelev *et al.* (ALICE Collaboration), Charged kaon femtoscopic correlations in *pp* collisions at $\sqrt{s} = 7$ TeV, arXiv:1212.5958 [hep-ex].
[56] A. Adare *et al.* (PHENIX Collaboration), Comparison of the space-time extent of the emission source in *d* + Au and Au + Au collisions at $\sqrt{s_{NN}} = 200$ GeV, arXiv:1404.5291 [nucl-ex].
[57] A. Adare, S. Afanasiev, C. Aidala, N. Ajitanand, and Y. Akiba, *et al.*, Beam-energy and system-size dependence of the space-time extent of the pion emission source produced in heavy-ion collisions, arXiv:1410.2559 [nucl-ex].
[58] P. Bozek and I. Wyskiel–Piekarska, Particle spectra in Pb-Pb collisions at $\sqrt{s_{NN}} = 2.76$ TeV, Phys. Rev. C **85**, 064915 (2012).

J. Adam,[40] D. Adamová,[83] M. M. Aggarwal,[87] G. Aglieri Rinella,[36] M. Agnello,[111] N. Agrawal,[48] Z. Ahammed,[132] S. U. Ahn,[68] I. Aimo,[94,111] S. Aiola,[137] M. Ajaz,[16] A. Akindinov,[58] S. N. Alam,[132] D. Aleksandrov,[100] B. Alessandro,[111] D. Alexandre,[102] R. Alfaro Molina,[64] A. Alici,[105,12] A. Alkin,[3] J. R. M. Almaraz,[119] J. Alme,[38] T. Alt,[43] S. Altinpinar,[18] I. Altsybeev,[131] C. Alves Garcia Prado,[120] C. Andrei,[78] A. Andronic,[97] V. Anguelov,[93] J. Anielski,[54] T. Antičić,[98] F. Antinori,[108] P. Antonioli,[105] L. Aphecetche,[113] H. Appelshäuser,[53] S. Arcelli,[28] N. Armesto,[17] R. Arnaldi,[111] I. C. Arsene,[22] M. Arslandok,[53] B. Audurier,[113] A. Augustinus,[36] R. Averbeck,[97] M. D. Azmi,[19] M. Bach,[43] A. Badalà,[107] Y. W. Baek,[44] S. Bagnasco,[111] R. Bailhache,[53] R. Bala,[90] A. Baldisseri,[15] F. Baltasar Dos Santos Pedrosa,[36] R. C. Baral,[61] A. M. Barbano,[111] R. Barbera,[29] F. Barile,[33] G. G. Barnaföldi,[136] L. S. Barnby,[102] V. Barret,[70] P. Bartalini,[7] K. Barth,[36] J. Bartke,[117] E. Bartsch,[53] M. Basile,[28] N. Bastid,[70] S. Basu,[132] B. Bathen,[54] G. Batigne,[113] A. Batista Camejo,[70] B. Batyunya,[66] P. C. Batzing,[22] I. G. Bearden,[80] H. Beck,[53] C. Bedda,[111] N. K. Behera,[49,48] I. Belikov,[55] F. Bellini,[28] H. Bello Martinez,[2] R. Bellwied,[122] R. Belmont,[135] E. Belmont-Moreno,[64] V. Belyaev,[76] G. Bencedi,[136] S. Beole,[27] I. Berceanu,[78] A. Bercuci,[78] Y. Berdnikov,[85] D. Berenyi,[136] R. A. Bertens,[57] D. Berzano,[36,27] L. Betev,[36] A. Bhasin,[90] I. R. Bhat,[90] A. K. Bhati,[87] B. Bhattacharjee,[45] J. Bhom,[128] L. Bianchi,[122] N. Bianchi,[72] C. Bianchin,[135,57] J. Bielčík,[40] J. Bielčíková,[83] A. Bilandzic,[80] R. Biswas,[4] S. Biswas,[79] S. Bjelogrlic,[57] J. T. Blair,[118] F. Blanco,[10] D. Blau,[100] C. Blume,[53] F. Bock,[93,74] A. Bogdanov,[76] H. Bøggild,[80] L. Boldizsár,[136] M. Bombara,[41] J. Book,[53] H. Borel,[15] A. Borissov,[96] M. Borri,[82] F. Bossú,[65] E. Botta,[27] S. Böttger,[52] P. Braun-Munzinger,[97] M. Bregant,[120] T. Breitner,[52] T. A. Broker,[53] T. A. Browning,[95] M. Broz,[40] E. J. Brucken,[46] E. Bruna,[111] G. E. Bruno,[33] D. Budnikov,[99] H. Buesching,[53] S. Bufalino,[27,111] P. Buncic,[36] O. Busch,[128,93] Z. Buthelezi,[65] J. B. Butt,[16] J. T. Buxton,[20] D. Caffarri,[36] X. Cai,[7] H. Caines,[137] L. Calero Diaz,[72] A. Caliva,[57] E. Calvo Villar,[103] P. Camerini,[26] F. Carena,[36] W. Carena,[36] F. Carnesecchi,[28] J. Castillo Castellanos,[15] A. J. Castro,[125] E. A. R. Casula,[25] C. Cavicchioli,[36] C. Ceballos Sanchez,[9] J. Cepila,[40] P. Cerello,[111] J. Cerkala,[115] B. Chang,[123] S. Chapeland,[36] M. Chartier,[124] J. L. Charvet,[15] S. Chattopadhyay,[132] S. Chattopadhyay,[101] V. Chelnokov,[3] M. Cherney,[86] C. Cheshkov,[130] B. Cheynis,[130] V. Chibante Barroso,[36] D. D. Chinellato,[121] P. Chochula,[36] K. Choi,[96] M. Chojnacki,[80] S. Choudhury,[132] P. Christakoglou,[81] C. H. Christensen,[80] P. Christiansen,[34] T. Chujo,[128] S. U. Chung,[96] Z. Chunhui,[57] C. Cicalo,[106] L. Cifarelli,[12,28] F. Cindolo,[105] J. Cleymans,[89] F. Colamaria,[33] D. Colella,[36,33,59] A. Collu,[25] M. Colocci,[28] G. Conesa Balbastre,[71] Z. Conesa del Valle,[51] M. E. Connors,[137] J. G. Contreras,[11,40] T. M. Cormier,[84] Y. Corrales Morales,[27] I. Cortés Maldonado,[2] P. Cortese,[32] M. R. Cosentino,[120] F. Costa,[36] P. Crochet,[70] R. Cruz Albino,[11] E. Cuautle,[63] L. Cunqueiro,[36] T. Dahms,[92,37] A. Dainese,[108] A. Danu,[62] D. Das,[101] I. Das,[51,101] S. Das,[4] A. Dash,[121] S. Dash,[48] S. De,[120] A. De Caro,[31,12] G. de Cataldo,[104] J. de Cuveland,[43] A. De Falco,[25] D. De Gruttola,[12,31] N. De Marco,[111] S. De Pasquale,[31] A. Deisting,[97,93] A. Deloff,[77] E. Dénes,[136] G. D'Erasmo,[33] D. Di Bari,[33] A. Di Mauro,[36] P. Di Nezza,[72] M. A. Diaz Corchero,[10] T. Dietel,[89] P. Dillenseger,[53] R. Divià,[36] Ø. Djuvsland,[18] A. Dobrin,[57,81] T. Dobrowolski,[77,*] D. Domenicis Gimenez,[120] B. Dönigus,[53] O. Dordic,[22] T. Drozhzhova,[53] A. K. Dubey,[132] A. Dubla,[57] L. Ducroux,[130] P. Dupieux,[70] R. J. Ehlers,[137] D. Elia,[104] H. Engel,[52] B. Erazmus,[36,113] I. Erdemir,[53] F. Erhardt,[129] D. Eschweiler,[43] B. Espagnon,[51] M. Estienne,[113] S. Esumi,[128] J. Eum,[96] D. Evans,[102] S. Evdokimov,[112] G. Eyyubova,[40] L. Fabbietti,[37,92] D. Fabris,[108] J. Faivre,[71] A. Fantoni,[72] M. Fasel,[74] L. Feldkamp,[54] D. Felea,[62] A. Feliciello,[111] G. Feofilov,[131]

J. Ferencei,[83] A. Fernández Téllez,[2] E. G. Ferreiro,[17] A. Ferretti,[27] A. Festanti,[30] V. J. G. Feuillard,[70,15] J. Figiel,[117] M. A. S. Figueredo,[124,120] S. Filchagin,[99] D. Finogeev,[56] E. M. Fiore,[33] M. G. Fleck,[93] M. Floris,[36] S. Foertsch,[65] P. Foka,[97] S. Fokin,[100] E. Fragiacomo,[110] A. Francescon,[30,36] U. Frankenfeld,[97] U. Fuchs,[36] C. Furget,[71] A. Furs,[56] M. Fusco Girard,[31] J. J. Gaardhøje,[80] M. Gagliardi,[27] A. M. Gago,[103] M. Gallio,[27] D. R. Gangadharan,[74] P. Ganoti,[88] C. Gao,[7] C. Garabatos,[97] E. Garcia-Solis,[13] C. Gargiulo,[36] P. Gasik,[92,37] M. Germain,[113] A. Gheata,[36] M. Gheata,[62,36] P. Ghosh,[132] S. K. Ghosh,[4] P. Gianotti,[72] P. Giubellino,[36,111] P. Giubilato,[30] E. Gladysz-Dziadus,[117] P. Glässel,[93] D. M. Goméz Coral,[64] A. Gomez Ramirez,[52] P. González-Zamora,[10] S. Gorbunov,[43] L. Görlich,[117] S. Gotovac,[116] V. Grabski,[64] L. K. Graczykowski,[134] K. L. Graham,[102] A. Grelli,[57] A. Grigoras,[36] C. Grigoras,[36] V. Grigoriev,[76] A. Grigoryan,[1] S. Grigoryan,[66] B. Grinyov,[3] N. Grion,[110] J. F. Grosse-Oetringhaus,[36] J.-Y. Grossiord,[130] R. Grosso,[36] F. Guber,[56] R. Guernane,[71] B. Guerzoni,[28] K. Gulbrandsen,[80] H. Gulkanyan,[1] T. Gunji,[127] A. Gupta,[90] R. Gupta,[90] R. Haake,[54] Ø. Haaland,[18] C. Hadjidakis,[51] M. Haiduc,[62] H. Hamagaki,[127] G. Hamar,[136] A. Hansen,[80] J. W. Harris,[137] H. Hartmann,[43] A. Harton,[13] D. Hatzifotiadou,[105] S. Hayashi,[127] S. T. Heckel,[53] M. Heide,[54] H. Helstrup,[38] A. Herghelegiu,[78] G. Herrera Corral,[11] B. A. Hess,[35] K. F. Hetland,[38] T. E. Hilden,[46] H. Hillemanns,[36] B. Hippolyte,[55] R. Hosokawa,[128] P. Hristov,[36] M. Huang,[18] T. J. Humanic,[20] N. Hussain,[45] T. Hussain,[19] D. Hutter,[43] D. S. Hwang,[21] R. Ilkaev,[99] I. Ilkiv,[77] M. Inaba,[128] M. Ippolitov,[76,100] M. Irfan,[19] M. Ivanov,[97] V. Ivanov,[85] V. Izucheev,[112] P. M. Jacobs,[74] S. Jadlovska,[115] C. Jahnke,[120] H. J. Jang,[68] M. A. Janik,[134] P. H. S. Y. Jayarathna,[122] C. Jena,[30] S. Jena,[122] R. T. Jimenez Bustamante,[97] P. G. Jones,[102] H. Jung,[44] A. Jusko,[102] P. Kalinak,[59] A. Kalweit,[36] J. Kamin,[53] J. H. Kang,[138] V. Kaplin,[76] S. Kar,[132] A. Karasu Uysal,[69] O. Karavichev,[56] T. Karavicheva,[56] L. Karayan,[93,97] E. Karpechev,[56] U. Kebschull,[52] R. Keidel,[139] D. L. D. Keijdener,[57] M. Keil,[36] K. H. Khan,[16] M. M. Khan,[19] P. Khan,[101] S. A. Khan,[132] A. Khanzadeev,[85] Y. Kharlov,[112] B. Kileng,[38] B. Kim,[138] D. W. Kim,[68,44] D. J. Kim,[123] H. Kim,[138] J. S. Kim,[44] M. Kim,[44] M. Kim,[138] S. Kim,[21] T. Kim,[138] S. Kirsch,[43] I. Kisel,[43] S. Kiselev,[58] A. Kisiel,[134] G. Kiss,[136] J. L. Klay,[6] C. Klein,[53] J. Klein,[36,93] C. Klein-Bösing,[54] A. Kluge,[36] M. L. Knichel,[93] A. G. Knospe,[118] T. Kobayashi,[128] C. Kobdaj,[114] M. Kofarago,[36] T. Kollegger,[43,97] A. Kolojvari,[131] V. Kondratiev,[131] N. Kondratyeva,[76] E. Kondratyuk,[112] A. Konevskikh,[56] M. Kopcik,[115] M. Kour,[90] C. Kouzinopoulos,[36] O. Kovalenko,[77] V. Kovalenko,[131] M. Kowalski,[117] G. Koyithatta Meethaleveedu,[48] J. Kral,[123] I. Králik,[59] A. Kravčáková,[41] M. Krelina,[40] M. Kretz,[43] M. Krivda,[102,59] F. Krizek,[83] E. Kryshen,[36] M. Krzewicki,[43] A. M. Kubera,[20] V. Kučera,[83] T. Kugathasan,[36] C. Kuhn,[55] P. G. Kuijer,[81] I. Kulakov,[43] A. Kumar,[90] J. Kumar,[48] L. Kumar,[79,87] P. Kurashvili,[77] A. Kurepin,[56] A. B. Kurepin,[56] A. Kuryakin,[99] S. Kushpil,[83] M. J. Kweon,[50] Y. Kwon,[138] S. L. La Pointe,[111] P. La Rocca,[29] C. Lagana Fernandes,[120] I. Lakomov,[36] R. Langoy,[42] C. Lara,[52] A. Lardeux,[15] A. Lattuca,[27] E. Laudi,[36] R. Lea,[26] L. Leardini,[93] G. R. Lee,[102] S. Lee,[138] I. Legrand,[36] F. Lehas,[81] R. C. Lemmon,[82] V. Lenti,[104] E. Leogrande,[57] I. León Monzón,[119] M. Leoncino,[27] P. Lévai,[136] S. Li,[7,70] X. Li,[14] J. Lien,[42] R. Lietava,[102] S. Lindal,[22] V. Lindenstruth,[43] C. Lippmann,[97] M. A. Lisa,[20] H. M. Ljunggren,[34] D. F. Lodato,[57] P. I. Loenne,[18] V. Loginov,[76] C. Loizides,[74] X. Lopez,[70] E. López Torres,[9] A. Lowe,[136] P. Luettig,[53] M. Lunardon,[30] G. Luparello,[26] P. H. F. N. D. Luz,[120] A. Maevskaya,[56] M. Mager,[36] S. Mahajan,[90] S. M. Mahmood,[22] A. Maire,[55] R. D. Majka,[137] M. Malaev,[85] I. Maldonado Cervantes,[63] L. Malinina,[66,†] D. Mal'Kevich,[58] P. Malzacher,[97] A. Mamonov,[99] V. Manko,[100] F. Manso,[70] V. Manzari,[36,104] M. Marchisone,[27] J. Mareš,[60] G. V. Margagliotti,[26] A. Margotti,[105] J. Margutti,[57] A. Marín,[97] C. Markert,[118] M. Marquard,[53] N. A. Martin,[97] J. Martin Blanco,[113] P. Martinengo,[36] M. I. Martínez,[2] G. Martínez García,[113] M. Martinez Pedreira,[36] Y. Martynov,[3] A. Mas,[120] S. Masciocchi,[97] M. Masera,[27] A. Masoni,[106] L. Massacrier,[113] A. Mastroserio,[33] H. Masui,[128] A. Matyja,[117] C. Mayer,[117] J. Mazer,[125] M. A. Mazzoni,[109] D. Mcdonald,[122] F. Meddi,[24] Y. Melikyan,[76] A. Menchaca-Rocha,[64] E. Meninno,[31] J. Mercado Pérez,[93] M. Meres,[39] Y. Miake,[128] M. M. Mieskolainen,[46] K. Mikhaylov,[58,66] L. Milano,[36] J. Milosevic,[22,133] L. M. Minervini,[104,23] A. Mischke,[57] A. N. Mishra,[49] D. Miśkowiec,[97] J. Mitra,[132] C. M. Mitu,[62] N. Mohammadi,[57] B. Mohanty,[132,79] L. Molnar,[55] L. Montaño Zetina,[11] E. Montes,[10] M. Morando,[30] D. A. Moreira De Godoy,[113,54] S. Moretto,[30] A. Morreale,[113] A. Morsch,[36] V. Muccifora,[72] E. Mudnic,[116] D. Mühlheim,[54] S. Muhuri,[132] M. Mukherjee,[132] J. D. Mulligan,[137] M. G. Munhoz,[120] S. Murray,[65] L. Musa,[36] J. Musinsky,[59] B. K. Nandi,[48] R. Nania,[105] E. Nappi,[104] M. U. Naru,[16] C. Nattrass,[125] K. Nayak,[79] T. K. Nayak,[132] S. Nazarenko,[99] A. Nedosekin,[58] L. Nellen,[63] F. Ng,[122] M. Nicassio,[97] M. Niculescu,[62,36] J. Niedziela,[36] B. S. Nielsen,[80] S. Nikolaev,[100] S. Nikulin,[100] V. Nikulin,[85] F. Noferini,[105,12] P. Nomokonov,[66] G. Nooren,[57] J. C. C. Noris,[2] J. Norman,[124] A. Nyanin,[100] J. Nystrand,[18] H. Oeschler,[93] S. Oh,[137] S. K. Oh,[67] A. Ohlson,[36] A. Okatan,[69] T. Okubo,[47] L. Olah,[136] J. Oleniacz,[134] A. C. Oliveira Da Silva,[120] M. H. Oliver,[137] J. Onderwaater,[97] C. Oppedisano,[111] R. Orava,[46] A. Ortiz Velasquez,[63] A. Oskarsson,[34] J. Otwinowski,[117] K. Oyama,[93] M. Ozdemir,[53] Y. Pachmayer,[93] P. Pagano,[31] G. Paić,[63] C. Pajares,[17] S. K. Pal,[132] J. Pan,[135] A. K. Pandey,[48] D. Pant,[48] P. Papcun,[115] V. Papikyan,[1] G. S. Pappalardo,[107] P. Pareek,[49] W. J. Park,[97] S. Parmar,[87] A. Passfeld,[54] V. Paticchio,[104] R. N. Patra,[132] B. Paul,[101] T. Peitzmann,[57] H. Pereira Da Costa,[15] E. Pereira De Oliveira Filho,[120] D. Peresunko,[100,76] C. E. Pérez Lara,[81] E. Perez Lezama,[53] V. Peskov,[53] Y. Pestov,[5] V. Petráček,[40] V. Petrov,[112] M. Petrovici,[78] C. Petta,[29] S. Piano,[110] M. Pikna,[39] P. Pillot,[113] O. Pinazza,[105,36] L. Pinsky,[122] D. B. Piyarathna,[122] M. Płoskoń,[74] M. Planinic,[129] J. Pluta,[134] S. Pochybova,[136] P. L. M. Podesta-Lerma,[119] M. G. Poghosyan,[86,84] B. Polichtchouk,[112] N. Poljak,[129] W. Poonsawat,[114] A. Pop,[78] S. Porteboeuf-Houssais,[70] J. Porter,[74] J. Pospisil,[83] S. K. Prasad,[4] R. Preghenella,[36,105] F. Prino,[111] C. A. Pruneau,[135] I. Pshenichnov,[56] M. Puccio,[111] G. Puddu,[25] P. Pujahari,[135] V. Punin,[99] J. Putschke,[135] H. Qvigstad,[22] A. Rachevski,[110] S. Raha,[4] S. Rajput,[90] J. Rak,[123] A. Rakotozafindrabe,[15] L. Ramello,[32] R. Raniwala,[91] S. Raniwala,[91] S. S. Räsänen,[46] B. T. Rascanu,[53] D. Rathee,[87] K. F. Read,[125] J. S. Real,[71] K. Redlich,[77] R. J. Reed,[135] A. Rehman,[18] P. Reichelt,[53] F. Reidt,[93,36] X. Ren,[7] R. Renfordt,[53]

A. R. Reolon,[72] A. Reshetin,[56] F. Rettig,[43] J.-P. Revol,[12] K. Reygers,[93] V. Riabov,[85] R. A. Ricci,[73] T. Richert,[34] M. Richter,[22] P. Riedler,[36] W. Riegler,[36] F. Riggi,[29] C. Ristea,[62] A. Rivetti,[111] E. Rocco,[57] M. Rodríguez Cahuantzi,[2] A. Rodriguez Manso,[81] K. Røed,[22] E. Rogochaya,[66] D. Rohr,[43] D. Röhrich,[18] R. Romita,[124] F. Ronchetti,[72] L. Ronflette,[113] P. Rosnet,[70] A. Rossi,[30,36] F. Roukoutakis,[88] A. Roy,[49] C. Roy,[55] P. Roy,[101] A. J. Rubio Montero,[10] R. Rui,[26] R. Russo,[27] E. Ryabinkin,[100] Y. Ryabov,[85] A. Rybicki,[117] S. Sadovsky,[112] K. Šafařík,[36] B. Sahlmuller,[53] P. Sahoo,[49] R. Sahoo,[49] S. Sahoo,[61] P. K. Sahu,[61] J. Saini,[132] S. Sakai,[72] M. A. Saleh,[135] C. A. Salgado,[17] J. Salzwedel,[20] S. Sambyal,[90] V. Samsonov,[85] X. Sanchez Castro,[55] L. Šándor,[59] A. Sandoval,[64] M. Sano,[128] D. Sarkar,[132] E. Scapparone,[105] F. Scarlassara,[30] R. P. Scharenberg,[95] C. Schiaua,[78] R. Schicker,[93] C. Schmidt,[97] H. R. Schmidt,[35] S. Schuchmann,[53] J. Schukraft,[36] M. Schulc,[40] T. Schuster,[137] Y. Schutz,[113,36] K. Schwarz,[97] K. Schweda,[97] G. Scioli,[28] E. Scomparin,[111] R. Scott,[125] J. E. Seger,[86] Y. Sekiguchi,[127] D. Sekihata,[47] I. Selyuzhenkov,[97] K. Senosi,[65] J. Seo,[96,67] E. Serradilla,[64,10] A. Sevcenco,[62] A. Shabanov,[56] A. Shabetai,[113] O. Shadura,[3] R. Shahoyan,[36] A. Shangaraev,[112] A. Sharma,[90] M. Sharma,[90] M. Sharma,[90] N. Sharma,[125,61] K. Shigaki,[47] K. Shtejer,[9,27] Y. Sibiriak,[100] S. Siddhanta,[106] K. M. Sielewicz,[36] T. Siemiarczuk,[77] D. Silvermyr,[84,34] C. Silvestre,[71] G. Simatovic,[129] G. Simonetti,[36] R. Singaraju,[132] R. Singh,[79] S. Singha,[132,79] V. Singhal,[132] B. C. Sinha,[132] T. Sinha,[101] B. Sitar,[39] M. Sitta,[32] T. B. Skaali,[22] M. Slupecki,[123] N. Smirnov,[137] R. J. M. Snellings,[57] T. W. Snellman,[123] C. Søgaard,[34] R. Soltz,[75] J. Song,[96] M. Song,[138] Z. Song,[7] F. Soramel,[30] S. Sorensen,[125] M. Spacek,[40] E. Spiriti,[72] I. Sputowska,[117] M. Spyropoulou-Stassinaki,[88] B. K. Srivastava,[95] J. Stachel,[93] I. Stan,[62] G. Stefanek,[77] M. Steinpreis,[20] E. Stenlund,[34] G. Steyn,[65] J. H. Stiller,[93] D. Stocco,[113] P. Strmen,[39] A. A. P. Suaide,[120] T. Sugitate,[47] C. Suire,[51] M. Suleymanov,[16] R. Sultanov,[58] M. Šumbera,[83] T. J. M. Symons,[74] A. Szabo,[39] A. Szanto de Toledo,[120,*] I. Szarka,[39] A. Szczepankiewicz,[36] M. Szymanski,[134] J. Takahashi,[121] G. J. Tambave,[18] N. Tanaka,[128] M. A. Tangaro,[33] J. D. Tapia Takaki,[51,‡] A. Tarantola Peloni,[53] M. Tarhini,[51] M. Tariq,[19] M. G. Tarzila,[78] A. Tauro,[36] G. Tejeda Muñoz,[2] A. Telesca,[36] K. Terasaki,[127] C. Terrevoli,[30,25] B. Teyssier,[130] J. Thäder,[74,97] D. Thomas,[118] R. Tieulent,[130] A. R. Timmins,[122] A. Toia,[53] S. Trogolo,[111] V. Trubnikov,[3] W. H. Trzaska,[123] T. Tsuji,[127] A. Tumkin,[99] R. Turrisi,[108] T. S. Tveter,[22] K. Ullaland,[18] A. Uras,[130] G. L. Usai,[25] A. Utrobicic,[129] M. Vajzer,[83] M. Vala,[59] L. Valencia Palomo,[70] S. Vallero,[27] J. Van Der Maarel,[57] J. W. Van Hoorne,[36] M. van Leeuwen,[57] T. Vanat,[83] P. Vande Vyvre,[36] D. Varga,[136] A. Vargas,[2] M. Vargyas,[123] R. Varma,[48] M. Vasileiou,[88] A. Vasiliev,[100] A. Vauthier,[71] V. Vechernin,[131] A. M. Veen,[57] M. Veldhoen,[57] A. Velure,[18] M. Venaruzzo,[73] E. Vercellin,[27] S. Vergara Limón,[2] R. Vernet,[8] M. Verweij,[135,36] L. Vickovic,[116] G. Viesti,[30,*] J. Viinikainen,[123] Z. Vilakazi,[126] O. Villalobos Baillie,[102] A. Vinogradov,[100] L. Vinogradov,[131] Y. Vinogradov,[99,*] T. Virgili,[31] V. Vislavicius,[34] Y. P. Viyogi,[132] A. Vodopyanov,[66] M. A. Völkl,[93] K. Voloshin,[58] S. A. Voloshin,[135] G. Volpe,[136,36] B. von Haller,[36] I. Vorobyev,[37,92] D. Vranic,[36,97] J. Vrláková,[41] B. Vulpescu,[70] A. Vyushin,[99] B. Wagner,[18] J. Wagner,[97] H. Wang,[57] M. Wang,[7,113] Y. Wang,[93] D. Watanabe,[128] Y. Watanabe,[127] M. Weber,[36] S. G. Weber,[97] J. P. Wessels,[54] U. Westerhoff,[54] J. Wiechula,[35] J. Wikne,[22] M. Wilde,[54] G. Wilk,[77] J. Wilkinson,[93] M. C. S. Williams,[105] B. Windelband,[93] M. Winn,[93] C. G. Yaldo,[135] H. Yang,[57] P. Yang,[7] S. Yano,[47] Z. Yin,[7] H. Yokoyama,[128] I.-K. Yoo,[96] V. Yurchenko,[3] I. Yushmanov,[100] A. Zaborowska,[134] V. Zaccolo,[80] A. Zaman,[16] C. Zampolli,[105] H. J. C. Zanoli,[120] S. Zaporozhets,[66] N. Zardoshti,[102] A. Zarochentsev,[131] P. Závada,[60] N. Zaviyalov,[99] H. Zbroszczyk,[134] I. S. Zgura,[62] M. Zhalov,[85] H. Zhang,[18,7] X. Zhang,[74] Y. Zhang,[7] C. Zhao,[22] N. Zhigareva,[58] D. Zhou,[7] Y. Zhou,[80,57] Z. Zhou,[18] H. Zhu,[18,7] J. Zhu,[113,7] X. Zhu,[7] A. Zichichi,[12,28] A. Zimmermann,[93] M. B. Zimmermann,[54,36] G. Zinovjev,[3] and M. Zyzak[43]

(ALICE Collaboration)

[1]*A. I. Alikhanyan National Science Laboratory (Yerevan Physics Institute) Foundation, Yerevan, Armenia*
[2]*Benemérita Universidad Autónoma de Puebla, Puebla, Mexico*
[3]*Bogolyubov Institute for Theoretical Physics, Kiev, Ukraine*
[4]*Bose Institute, Department of Physics and Centre for Astroparticle Physics and Space Science (CAPSS), Kolkata, India*
[5]*Budker Institute for Nuclear Physics, Novosibirsk, Russia*
[6]*California Polytechnic State University, San Luis Obispo, California, United States*
[7]*Central China Normal University, Wuhan, China*
[8]*Centre de Calcul de l'IN2P3, Villeurbanne, France*
[9]*Centro de Aplicaciones Tecnológicas y Desarrollo Nuclear (CEADEN), Havana, Cuba*
[10]*Centro de Investigaciones Energéticas Medioambientales y Tecnológicas (CIEMAT), Madrid, Spain*
[11]*Centro de Investigación y de Estudios Avanzados (CINVESTAV), Mexico City and Mérida, Mexico*
[12]*Centro Fermi–Museo Storico della Fisica e Centro Studi e Ricerche "Enrico Fermi," Rome, Italy*
[13]*Chicago State University, Chicago, Illinois, USA*
[14]*China Institute of Atomic Energy, Beijing, China*
[15]*Commissariat à l'Energie Atomique, IRFU, Saclay, France*
[16]*COMSATS Institute of Information Technology (CIIT), Islamabad, Pakistan*
[17]*Departamento de Física de Partículas and IGFAE, Universidad de Santiago de Compostela, Santiago de Compostela, Spain*
[18]*Department of Physics and Technology, University of Bergen, Bergen, Norway*
[19]*Department of Physics, Aligarh Muslim University, Aligarh, India*
[20]*Department of Physics, Ohio State University, Columbus, Ohio, United States*

[21]*Department of Physics, Sejong University, Seoul, South Korea*
[22]*Department of Physics, University of Oslo, Oslo, Norway*
[23]*Dipartimento di Elettrotecnica ed Elettronica del Politecnico, Bari, Italy*
[24]*Dipartimento di Fisica dell'Università 'La Sapienza' and Sezione INFN Rome, Italy*
[25]*Dipartimento di Fisica dell'Università and Sezione INFN, Cagliari, Italy*
[26]*Dipartimento di Fisica dell'Università and Sezione INFN, Trieste, Italy*
[27]*Dipartimento di Fisica dell'Università and Sezione INFN, Turin, Italy*
[28]*Dipartimento di Fisica e Astronomia dell'Università and Sezione INFN, Bologna, Italy*
[29]*Dipartimento di Fisica e Astronomia dell'Università and Sezione INFN, Catania, Italy*
[30]*Dipartimento di Fisica e Astronomia dell'Università and Sezione INFN, Padova, Italy*
[31]*Dipartimento di Fisica 'E. R. Caianiello' dell'Università and Gruppo Collegato INFN, Salerno, Italy*
[32]*Dipartimento di Scienze e Innovazione Tecnologica dell'Università del Piemonte Orientale and Gruppo Collegato INFN, Alessandria, Italy*
[33]*Dipartimento Interateneo di Fisica 'M. Merlin' and Sezione INFN, Bari, Italy*
[34]*Division of Experimental High Energy Physics, University of Lund, Lund, Sweden*
[35]*Eberhard Karls Universität Tübingen, Tübingen, Germany*
[36]*European Organization for Nuclear Research (CERN), Geneva, Switzerland*
[37]*Excellence Cluster Universe, Technische Universität München, Munich, Germany*
[38]*Faculty of Engineering, Bergen University College, Bergen, Norway*
[39]*Faculty of Mathematics, Physics and Informatics, Comenius University, Bratislava, Slovakia*
[40]*Faculty of Nuclear Sciences and Physical Engineering, Czech Technical University in Prague, Prague, Czech Republic*
[41]*Faculty of Science, P. J. Šafárik University, Košice, Slovakia*
[42]*Faculty of Technology, Buskerud and Vestfold University College, Vestfold, Norway*
[43]*Frankfurt Institute for Advanced Studies, Johann Wolfgang Goethe-Universität Frankfurt, Frankfurt, Germany*
[44]*Gangneung–Wonju National University, Gangneung, South Korea*
[45]*Gauhati University, Department of Physics, Guwahati, India*
[46]*Helsinki Institute of Physics (HIP), Helsinki, Finland*
[47]*Hiroshima University, Hiroshima, Japan*
[48]*Indian Institute of Technology Bombay (IIT), Mumbai, India*
[49]*Indian Institute of Technology Indore, Indore (IITI), India*
[50]*Inha University, Incheon, South Korea*
[51]*Institut de Physique Nucléaire d'Orsay (IPNO), Université Paris-Sud, CNRS-IN2P3, Orsay, France*
[52]*Institut für Informatik, Johann Wolfgang Goethe-Universität Frankfurt, Frankfurt, Germany*
[53]*Institut für Kernphysik, Johann Wolfgang Goethe-Universität Frankfurt, Frankfurt, Germany*
[54]*Institut für Kernphysik, Westfälische Wilhelms-Universität Münster, Münster, Germany*
[55]*Institut Pluridisciplinaire Hubert Curien (IPHC), Université de Strasbourg, CNRS-IN2P3, Strasbourg, France*
[56]*Institute for Nuclear Research, Academy of Sciences, Moscow, Russia*
[57]*Institute for Subatomic Physics of Utrecht University, Utrecht, Netherlands*
[58]*Institute for Theoretical and Experimental Physics, Moscow, Russia*
[59]*Institute of Experimental Physics, Slovak Academy of Sciences, Košice, Slovakia*
[60]*Institute of Physics, Academy of Sciences of the Czech Republic, Prague, Czech Republic*
[61]*Institute of Physics, Bhubaneswar, India*
[62]*Institute of Space Science (ISS), Bucharest, Romania*
[63]*Instituto de Ciencias Nucleares, Universidad Nacional Autónoma de México, Mexico City, Mexico*
[64]*Instituto de Física, Universidad Nacional Autónoma de México, Mexico City, Mexico*
[65]*iThemba LABS, National Research Foundation, Somerset West, South Africa*
[66]*Joint Institute for Nuclear Research (JINR), Dubna, Russia*
[67]*Konkuk University, Seoul, South Korea*
[68]*Korea Institute of Science and Technology Information, Daejeon, South Korea*
[69]*KTO Karatay University, Konya, Turkey*
[70]*Laboratoire de Physique Corpusculaire (LPC), Clermont Université, Université Blaise Pascal, CNRS–IN2P3, Clermont-Ferrand, France*
[71]*Laboratoire de Physique Subatomique et de Cosmologie, Université Grenoble-Alpes, CNRS-IN2P3, Grenoble, France*
[72]*Laboratori Nazionali di Frascati, INFN, Frascati, Italy*
[73]*Laboratori Nazionali di Legnaro, INFN, Legnaro, Italy*
[74]*Lawrence Berkeley National Laboratory, Berkeley, California, United States*
[75]*Lawrence Livermore National Laboratory, Livermore, California, United States*
[76]*Moscow Engineering Physics Institute, Moscow, Russia*
[77]*National Centre for Nuclear Studies, Warsaw, Poland*

[78] *National Institute for Physics and Nuclear Engineering, Bucharest, Romania*
[79] *National Institute of Science Education and Research, Bhubaneswar, India*
[80] *Niels Bohr Institute, University of Copenhagen, Copenhagen, Denmark*
[81] *Nikhef, Nationaal instituut voor subatomaire fysica, Amsterdam, Netherlands*
[82] *Nuclear Physics Group, STFC Daresbury Laboratory, Daresbury, United Kingdom*
[83] *Nuclear Physics Institute, Academy of Sciences of the Czech Republic, Řež u Prahy, Czech Republic*
[84] *Oak Ridge National Laboratory, Oak Ridge, Tennessee, United States*
[85] *Petersburg Nuclear Physics Institute, Gatchina, Russia*
[86] *Physics Department, Creighton University, Omaha, Nebraska, United States*
[87] *Physics Department, Panjab University, Chandigarh, India*
[88] *Physics Department, University of Athens, Athens, Greece*
[89] *Physics Department, University of Cape Town, Cape Town, South Africa*
[90] *Physics Department, University of Jammu, Jammu, India*
[91] *Physics Department, University of Rajasthan, Jaipur, India*
[92] *Physik Department, Technische Universität München, Munich, Germany*
[93] *Physikalisches Institut, Ruprecht–Karls-Universität Heidelberg, Heidelberg, Germany*
[94] *Politecnico di Torino, Turin, Italy*
[95] *Purdue University, West Lafayette, Indiana, United States*
[96] *Pusan National University, Pusan, South Korea*
[97] *Research Division and ExtreMe Matter Institute EMMI, GSI Helmholtzzentrum für Schwerionenforschung, Darmstadt, Germany*
[98] *Rudjer Bošković Institute, Zagreb, Croatia*
[99] *Russian Federal Nuclear Center (VNIIEF), Sarov, Russia*
[100] *Russian Research Centre Kurchatov Institute, Moscow, Russia*
[101] *Saha Institute of Nuclear Physics, Kolkata, India*
[102] *School of Physics and Astronomy, University of Birmingham, Birmingham, United Kingdom*
[103] *Sección Física, Departamento de Ciencias, Pontificia Universidad Católica del Perú, Lima, Peru*
[104] *Sezione INFN, Bari, Italy*
[105] *Sezione INFN, Bologna, Italy*
[106] *Sezione INFN, Cagliari, Italy*
[107] *Sezione INFN, Catania, Italy*
[108] *Sezione INFN, Padova, Italy*
[109] *Sezione INFN, Rome, Italy*
[110] *Sezione INFN, Trieste, Italy*
[111] *Sezione INFN, Turin, Italy*
[112] *SSC IHEP of NRC Kurchatov institute, Protvino, Russia*
[113] *SUBATECH, Ecole des Mines de Nantes, Université de Nantes, CNRS-IN2P3, Nantes, France*
[114] *Suranaree University of Technology, Nakhon Ratchasima, Thailand*
[115] *Technical University of Košice, Košice, Slovakia*
[116] *Technical University of Split FESB, Split, Croatia*
[117] *The Henryk Niewodniczanski Institute of Nuclear Physics, Polish Academy of Sciences, Cracow, Poland*
[118] *The University of Texas at Austin, Physics Department, Austin, Texas, USA*
[119] *Universidad Autónoma de Sinaloa, Culiacán, Mexico*
[120] *Universidade de São Paulo (USP), São Paulo, Brazil*
[121] *Universidade Estadual de Campinas (UNICAMP), Campinas, Brazil*
[122] *University of Houston, Houston, Texas, United States*
[123] *University of Jyväskylä, Jyväskylä, Finland*
[124] *University of Liverpool, Liverpool, United Kingdom*
[125] *University of Tennessee, Knoxville, Tennessee, United States*
[126] *University of the Witwatersrand, Johannesburg, South Africa*
[127] *University of Tokyo, Tokyo, Japan*
[128] *University of Tsukuba, Tsukuba, Japan*
[129] *University of Zagreb, Zagreb, Croatia*
[130] *Université de Lyon, Université Lyon 1, CNRS/IN2P3, IPN-Lyon, Villeurbanne, France*
[131] *V. Fock Institute for Physics, St. Petersburg State University, St. Petersburg, Russia*
[132] *Variable Energy Cyclotron Centre, Kolkata, India*
[133] *Vinča Institute of Nuclear Sciences, Belgrade, Serbia*
[134] *Warsaw University of Technology, Warsaw, Poland*
[135] *Wayne State University, Detroit, Michigan, United States*

[136] *Wigner Research Centre for Physics, Hungarian Academy of Sciences, Budapest, Hungary*
[137] *Yale University, New Haven, Connecticut, United States*
[138] *Yonsei University, Seoul, South Korea*
[139] *Zentrum für Technologietransfer und Telekommunikation (ZTT), Fachhochschule Worms, Worms, Germany*

[*] Deceased.
[†] Also at M. V. Lomonosov Moscow State University, D. V. Skobeltsyn Institute of Nuclear, Physics, Moscow, Russia.
[‡] Also at University of Kansas, Lawrence, Kansas, USA.